

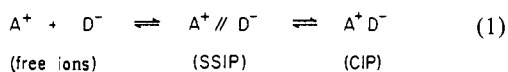
Charge-Transfer Ion Pairs. Structure and Photoinduced Electron Transfer of Carbonylmetalate Salts

T. M. Bockman and J. K. Kochi*

Contribution from the Department of Chemistry, University of Houston, University Park, Houston, Texas 77204-5641. Received December 15, 1988

Abstract: Brightly colored crystals, readily isolated from such colorless carbonylmetalates as $\text{Co}(\text{CO})_4^-$, $\text{Mn}(\text{CO})_5^-$, and $\text{V}(\text{CO})_6^-$ in conjunction with various metallocenium and pyridinium cations, are identified as charge-transfer (CT) salts by their unambiguous absorption and diffuse reflectance spectra. X-ray crystallography of such CT salts establishes the relevant interionic separations, the spatial cation/anion orientations, as well as the deviations from tetrahedral $\text{Co}(\text{CO})_4^-$ configuration that are all inherent to the charge-transfer interaction of intimate ion pairs. The $\text{Co}(\text{CO})_4^-$ distortions, as observed in the crystal structures, are also revealed by their characteristic carbonyl IR spectra. The persistence of the unique carbonyl IR and charge-transfer absorption bands in nonpolar solvents thus leads to contact ion pairs (CIP) that are closely related or structurally the same as those elucidated by X-ray crystallography. Accordingly, the charge-transfer excitation of contact ion pairs can be examined directly in solution by time-resolved spectroscopy. The spectral observation of the radical pair $[\text{Cp}_2\text{Co}^+\text{Mn}(\text{CO})_5^-]$ from the 532-nm excitation of the charge-transfer salt $[\text{Cp}_2\text{Co}^+\text{Mn}(\text{CO})_5^-]$ with a 10-ns laser pulse represents the experimental verification of Mulliken theory. As such, the efficient scavenging of such labile 17-electron carbonylmetal radicals as $\text{Co}(\text{CO})_4^*$ and $\text{Mn}(\text{CO})_5^*$ affords a rich menu of productive photochemistry attendant upon the charge-transfer excitation of contact ion pairs.

Intermolecular interaction of ions has been roughly categorized in terms of contact ion pairs (CIP) and solvent-separated ion pairs (SSIP)¹⁻⁴



though doubtlessly a myriad of ion-pair types exist with continuously varying interionic separations. Of these, only the contact ion pair is the critical precursor to electrophile/nucleophile interactions.⁵⁻⁹ Unfortunately there are no techniques to establish CIP structures in solution, such as those routinely available for solids and gases.¹⁰

Electronic transitions of electron donor-acceptor complexes from both neutral and charged components have been delineated as charge-transfer (CT) excitations by Mulliken.^{11,12} The characteristic charge-transfer absorption bands have been identified in various pyridinium iodides that are constituted as acceptor/donor contact ion pairs in solution.¹³ Charge-transfer

bands have also been reported for carbonylmetalate salts such as $\text{Ti}^+\text{Co}(\text{CO})_4^-$,¹⁴ $\text{py}^+\text{V}(\text{CO})_6^-$,¹⁵ and $\text{Co}(\text{CO})_3\text{L}_2^+\text{Co}(\text{CO})_4^-$ ¹⁶ where py^+ = pyridinium cations and L = phosphines. Indeed, we believe that the strong and variable donor properties of carbonylmetalates¹⁷ can be exploited in the quantitative study of contact ion pairs by the close examination of their charge-transfer characteristics. Accordingly, we prepared a series of carbonylmetalate salts and have established their structures by X-ray crystallography. In this report we demonstrate how the crystallographic structures can be related to contact ion pairs in solution. Furthermore, we show how the unique properties of anionic carbonylmetalate donors lead to CT excited states that result in a wide variety of productive photochemistry.¹⁸

Results

The ion pairs in this study comprised three series of colorless carbonylmetalate anions, viz., tetracarbonylcobaltate $[\text{Co}(\text{CO})_4^-]$, hexacarbonylvanadate $[\text{V}(\text{CO})_6^-]$, and pentacarbonylmanganate $[\text{Mn}(\text{CO})_5^-]$, together with iodide, that were prepared as the sodium or PPN salts.¹⁹⁻²¹ Moreover, three distinct classes of colorless acceptor cations, viz., cobaltocenium (Cp_2Co^+),²² dibenzenechromium $[(\text{C}_6\text{H}_6)_2\text{Cr}^+]$,²³ and a series of *N*-methylpyridinium²⁴ derivatives were synthesized as either the halide or hexafluorophosphate salt (see Experimental Section).

I. Isolation and Spectral Characterization of Charge-Transfer Salts of Carbonylmetalates. When a pair of colorless aqueous solutions containing 0.1 M $\text{Na}^+\text{Co}(\text{CO})_4^-$ and $\text{Cp}_2\text{Co}^+\text{Cl}^-$ was poured together, dark red crystals separated immediately. This

(1) Fuoss, R. M.; Accascina, F. *Electrolytic Conductance*; Wiley: New York, 1959.

(2) Davis, C. W. *Ion Association*; Butterworth: London, 1962.

(3) Szwarc, M., Ed. *Ions and Ion Pairs in Organic Reactions*; Wiley: New York, 1972; 1974; Vol. 1 and 2.

(4) Gordon, J. E. *Organic Chemistry of Electrolyte Solutions*; Wiley: New York, 1975.

(5) For example, see: (a) Cordes, E. H.; Dunlap, R. B. *Acc. Chem. Res.* **1969**, *2*, 329. (b) Kessler, H.; Feigel, M. *Acc. Chem. Res.* **1982**, *15*, 2.

(6) Troughton, E. B.; Molter, K. E.; Arnett, E. M. *J. Am. Chem. Soc.* **1984**, *106*, 6726.

(7) (a) Hughes, E. D.; Ingold, C. K. *J. Chem. Soc.* **1935**, 244. (b) Hughes, E. D.; Ingold, C. K.; Patel, C. S. *J. Chem. Soc.* **1933**, 526. (c) Ingold, C. K. *Structure and Mechanism in Organic Chemistry*; 2nd ed.; Cornell University: Ithaca, NY, 1969.

(8) For the microscopic reverse, see: (a) Winstein, S.; Robinson, G. C. *J. Am. Chem. Soc.* **1958**, *80*, 169. (b) Winstein, S.; Clippinger, E.; Fainberg, A. H.; Robinson, G. C. *J. Am. Chem. Soc.* **1954**, *76*, 2597.

(9) Harris, J. M. *Prog. Phys. Org. Chem.* **1974**, *11*, 89. Shiner, V. J., Jr. In *Isotopes Effects in Chemical Reactions*; Collin, C. J., Bowman, N. S., Eds.; Van Nostrand: New York, 1970.

(10) (a) Stout, G. H.; Jensen, L. H. *X-ray Structure Determination: A Practical Guide*; MacMillan: New York, 1968. (b) Jeffrey, J. W. *Methods in X-ray Crystallography*; Academic: New York, 1971. (c) Hagen, K.; Holwill, C. J.; Rice, D. J.; Runnacles, J. D. *Inorg. Chem.* **1988**, *27*, 2032, and references therein. (d) See, however, the recent solution XDS studies of ion pairing by: Licheri, G.; Paschina, G.; Piccaluga, G.; Pinna, G. *J. Chem. Phys.* **1984**, *81*, 6059. Caminiti, R. *J. Chem. Phys.* **1986**, *84*, 3336.

(11) Mulliken, R. S. *J. Am. Chem. Soc.* **1952**, *74*, 811.

(12) Mulliken, R. S.; Person, W. B. *Molecular Complexes: A Reprint and Lecture Volume*; Wiley: New York, 1969.

(13) (a) Kosower, E. M. *J. Am. Chem. Soc.* **1958**, *80*, 3253. (b) Kosower, E. M.; Skorcz, J. A. *J. Am. Chem. Soc.* **1960**, *82*, 2195. (c) Kosower, E. M.; Mohammad, M. J. *Phys. Chem.* **1970**, *74*, 1153.

(14) Schramm, C.; Zink, J. I. *J. Am. Chem. Soc.* **1979**, *101*, 4554. See also: Pedersen, S. E.; Robinson, W. R. *Inorg. Chem.* **1975**, *14*, 2360.

(15) (a) Calderazzo, F.; Pampaloni, G.; Lanfranchi, M.; Pelizzi, G. *J. Organomet. Chem.* **1985**, *296*, 1. (b) Calderazzo, F.; Pampaloni, G.; Pelizzi, G.; Vitali, F. *Organometallics* **1988**, *7*, 1083.

(16) Volger, A.; Kunkely, H. *Organometallics* **1988**, *7*, 1449.

(17) Geiger, W. E.; Connelly, N. G. *Adv. Organomet. Chem.* **1984**, *23*, 1.

(18) For related photoredox processes, see: (a) Fox, M. A. *Adv. Photochem.* **1986**, *13*, 237. (b) Kavarnos, G. J.; Turro, N. J. *Chem. Rev.* **1986**, *86*, 401. (c) Mattay, J. *Angew. Chem., Int. Ed. Engl.* **1987**, *26*, 825. (d) Hennig, H.; Rehorek, D.; Archer, R. D. *Coord. Chem. Rev.* **1985**, *61*, 1. (e) For a preliminary report, see: Bockman, T. M.; Kochi, J. K. *J. Am. Chem. Soc.* **1988**, *110*, 1294.

(19) Schussler, D. P.; Robinson, W. R.; Edgell, W. F. *Inorg. Chem.* **1974**, *13*, 153. See also: Reference 14.

(20) Rehder, D. *J. Organomet. Chem.* **1972**, *37*, 303.

(21) (a) Faltynsek, R. A.; Wrighton, M. S. *J. Am. Chem. Soc.* **1978**, *100*, 2701. (b) PPN = bis(triphenylphosphoranylidene)ammonium, $(\text{Ph}_3\text{P})_2\text{N}^+$.

(22) Sohn, Y. S.; Hendrickson, D. N.; Gray, H. B. *J. Am. Chem. Soc.* **1971**, *93*, 3603.

(23) Fischer, E. O.; Scherer, F.; Stahl, H. O. *Chem. Ber.* **1960**, *93*, 2065.

(24) See: Vogel, A. I. *Textbook of Practical Organic Chemistry*; Wiley: New York, 1956.

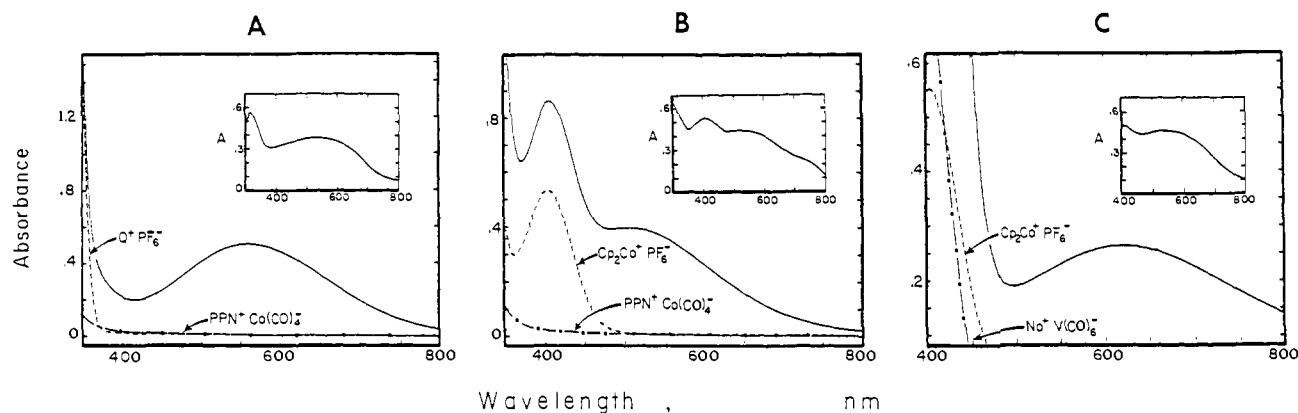


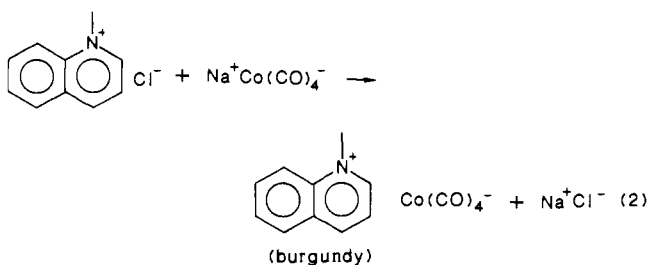
Figure 1. Charge-transfer absorption spectra of (A) $Q^+Co(CO)_4^-$, (B) $Cp_2Co^+Co(CO)_4^-$, and (C) $Cp_2Co^+V(CO)_6^-$ as 10^{-3} M solutions in CH_2Cl_2 , together with the absorption spectra of the separate cationic acceptor (---) and the anionic donor (---) at the same concentration. The diffuse reflectance spectra of the corresponding crystalline salts (10%) dispersed in silica are shown in the insets.

Table I. Visible Absorption Bands of Charge-Transfer Salts in the Crystalline Solid State and in Solution^a

cationic acceptor ^c	E_c (V vs SCE) ^d	anionic donor ^b			
		$Co(CO)_4^-$	$V(CO)_6^-$	$Mn(CO)_5^-$	I^-
PP ⁺	(-1.27)	442 (494)	512 (578)	(562) ^f	(<380) (390)
Cp_2Co^+	(-0.99)	508 (520)	540 (630)	600 (570) ^e	
iQ ⁺	(-1.08)	510 (516)		(580) ^f	
Q ⁺	(-0.90)	520 (550)	520 (720)		465 (444)
$(C_6H_6)_2Cr^+$		516			
CMP ⁺	(-0.79)	(590) ^f	600 (760)	(642) ^f	490 (454)
NCP ⁺	(-0.67)	560 (620) ^f			

^a Maximum (nm) of the electronic band obtained from the diffuse reflectance spectrum after 10% dispersion in silica. ^b Absorption spectrum in 10^{-3} M dichloromethane solution in parentheses. ^c For identification of the acronym, see ref 28. ^d Irreversible cathodic CV peak potential at 500 mV s^{-1} . ^e Prepared in situ from Na⁺ salt. ^f Prepared in situ from PPN⁺ salt.

remarkable visual display was also observed when an aqueous solution of $Na^+Co(CO)_4^-$ was mixed with colorless saline solutions of cyanopyridinium (NCP⁺), quinolinium (Q⁺), phenylpyridinium (PP⁺), and dibenzenechromium [$(C_6H_6)_2Cr^+$] chlorides to yield dark blue, burgundy, orange, and green crystals, respectively.



Analogously, when a colorless aqueous solution of quinolinium chloride (Q^+Cl^-) was mixed with an almost colorless aqueous solution of $Na^+V(CO)_6^-$, the well-formed dark green crystals of the vanadate salt precipitated immediately. In each case, the spontaneous separation of the highly colored salts was made even more dramatic by the absence of color in the aqueous mother liquors throughout the course of precipitation.

The quantitative effects in these colored salts are illustrated in Figure 1 by the appearance of broad absorption bands in the spectral region from 350 to beyond 700 nm when they were dissolved in dichloromethane. For comparison, the inset in each of the figures shows the diffuse reflectance spectrum of the crystalline salt.²⁵ The correspondence of the band maximum (λ_{CT}) and breadth (fwhm) of the absorption and reflectance spectra indicated the close similarity of the various carbonylcobaltate salts dissolved in solution to those in the crystalline solid state, respectively (Table I).²⁶ Analogously, the absorption bands of the

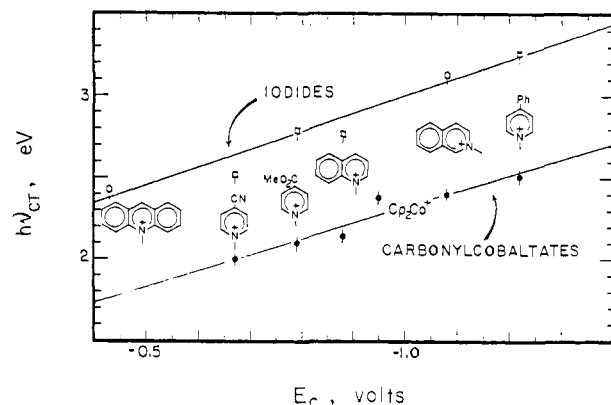


Figure 2. Correlation of the charge-transfer absorption bands ($h\nu_{CT}$) of carbonylcobalt (●) and iodide (□) salts with the reduction potentials E_c of various pyridinium cations.

various iodide salts in dichloromethane solution were also similar to those in the solid state (Table I).

The absorption bands listed in Table I showed two important trends. For the series of carbonylcobaltate salts, the maximum λ_{CT} s were consistently red-shifted with cation variation in the following order: $PP^+ > Cp_2Co^+ > Q^+ > (C_6H_6)_2Cr^+ > NCP^+$. Furthermore, the same order applied to the corresponding carbonylvandate, carbonylmanganate, and iodide salts. Such a progressive bathochromic shift of the absorption bands ($h\nu_{CT}$) with the decreasing cathodic potentials E_c for cation reduction (as viewed down the rows in Table I)²⁷ is illustrated in Figure 2.²⁸

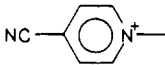
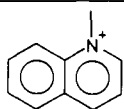
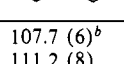
(27) E_c and E_a represent the cathodic and anodic peak potentials for the irreversible 1-electron cyclic voltammetric waves of acceptor cations and donor anions, respectively, as described in the Experimental Section.

(28) Specifically, NCP⁺ = 4-cyano-*N*-methylpyridinium, Q⁺ = *N*-methyl-1-quinolinium, PP⁺ = 4-phenyl-*N*-methylpyridinium, iQ⁺ = *N*-methyl-2-quinolinium, CMP⁺ = 4-carbomethoxy-*N*-pyridinium, NCP⁺ = 4-cyano-*N*-methylpyridinium, generally isolated and used as the iodide or chloride salts.

(25) As a $\sim 10\%$ mixture obtained by grinding with silica (100 mesh).

(26) The band maximums (λ_{CT}) obtained from the absorption spectra in dichloromethane solution are generally red-shifted relative to that of the diffuse reflectance spectrum of the crystalline salt.

Table II. Bond Angles and Bond Distances for $\text{Co}(\text{CO})_4^-$ in Charge-Transfer Salts

Å/deg	Cp_2Co^+		NC— 
			
C—Co—C	106.7 (4) ^a 110.8 (4)	107.7 (6) ^b 111.2 (8)	107.5 (5) ^{c,d} 113.0 (3)
Co—O	1.791 (6) 1.779 (6)	1.747 (5) 1.755 (4)	1.763 (9) ^{c,d} 1.772 (9)
C—O	1.135 (6) 1.138 (6)	1.151 (4) 1.157 (5)	1.151 (8) 1.134 (9)

^aTetracarbonylcobaltate in C_{2v} symmetry. ^bTetracarbonylcobaltate in C_{3v} symmetry. ^cTetracarbonylcobaltate in C_s symmetry. ^dFor other parameters, see Supplementary Material.

The pair of lines in the figure describe the slope of unity for the linear correlation given by

$$h\nu_{\text{CT}} = -aE_c + \text{constant} \quad (3)$$

with $a = 1.00$ for both series of carbonylcobaltate and iodide salts. According to Mulliken charge-transfer theory,^{11,12} the separation of $\Delta h\nu_{\text{CT}} = 0.61$ eV for the two series represents the constant difference in the donor properties (ionization potential) of $\text{Co}(\text{CO})_4^-$ and I^- in salt pairs with the same acceptor cation. The latter is a corollary of the Mulliken relationship for a series of carbonylmetalate salts in which the charge-transfer maximums viewed across the columns in Table I were consistently blue-shifted in the order $\text{Mn}(\text{CO})_5^- \lesssim \text{V}(\text{CO})_6^- < \text{Co}(\text{CO})_4^- < \text{I}^-$. Indeed, such a progressive increase in the energy of the absorption bands with the increasing anodic potential E_a for anion oxidation²⁹ represents the linear correlation

$$h\nu_{\text{CT}} = bE_a + \text{constant} \quad (4)$$

that applies to salts derived from a common cation and a series of donor anions. The linear correlations in eq 3 and 4 derive from Mulliken theory, more commonly expressed as³⁰

$$h\nu_{\text{CT}} = I_D - E_A + \omega + \text{constant} \quad (5)$$

where I_D and E_A are the ionization potential and electron affinity of the donor anions and acceptor cations, respectively, in the gas phase and ω represents the ion-pair interaction.³¹ Accordingly, we will refer to these colored crystals interchangeably as charge-transfer salts in all further discussions.³²

II. X-ray Crystallographic Structures of Charge-Transfer Salts.

To establish the origin of the charge-transfer absorptions of the colored salts in Table I, we examined the X-ray crystallography of the tetracarbonylcobaltate salts of the representative cations Cp_2Co^+ , Q^+ , and NCP^+ —together with $\text{Cp}_2\text{Co}^+\text{I}^-$ and $\text{Cp}_2\text{Co}^+\text{V}(\text{CO})_6^-$ for comparison. The X-ray diffraction patterns from $\text{Cp}_2\text{Co}^+\text{Co}(\text{CO})_4^-$, $\text{Q}^+\text{Co}(\text{CO})_4^-$, and $\text{NCP}^+\text{Co}(\text{CO})_4^-$ as deep red, burgundy, and blue crystals were all solved as the expected 1:1 ion pairs (see Experimental Section). In each salt, the tetracarbonylcobaltate moiety was present as a discrete tetrahedral anion with a slight distortion from ideal T_d symmetry. The corresponding bond angles for $\text{Co}(\text{CO})_4^-$ are listed in Table II, together with the critical bond distances. Indeed, these structural parameters, with only slight variations, were the same as those previously found in the colorless ionic salts of tetracarbonylcobaltate paired with alkali^{33,34} and simple ammonium cations.³⁵

(29) E_a for $\text{Mn}(\text{CO})_5^-$, $\text{V}(\text{CO})_6^-$, $\text{Co}(\text{CO})_4^-$, and I^- are -0.11 , 0.06 , 0.33 , and 0.36 V vs SCE at a scan rate of $\nu = 500$ mV s^{-1} .

(30) Hanna, M. W.; Lippert, J. L. *Molecular Complexes*; Foster, R., Ed.; Elek Science: London, 1973; Vol. 1, p 1ff.

(31) (a) The differences between I_D and E_A in the gas phase (eq 5) with E_a and E_c in solution (eq 3 and 4) are largely covered by solvation. (b) For Coulombic interactions, $\omega = e^2/r_{A+D}$.

(32) See: Foster, R. *Organic Charge-Transfer Complexes*; Academic: New York, 1969.

(33) Klüfers, P. Z. *Kristallogr.* **1984**, *167*, 275.

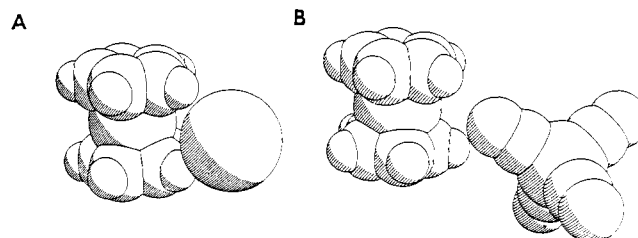


Figure 3. Space-filling models of (A) $\text{Cp}_2\text{Co}^+\text{I}^-$ and (B) $\text{Cp}_2\text{Co}^+\text{Co}(\text{CO})_4^-$ based on X-ray crystallography showing the location of the anionic donors in the equatorial plane of the cobalticenium cation.

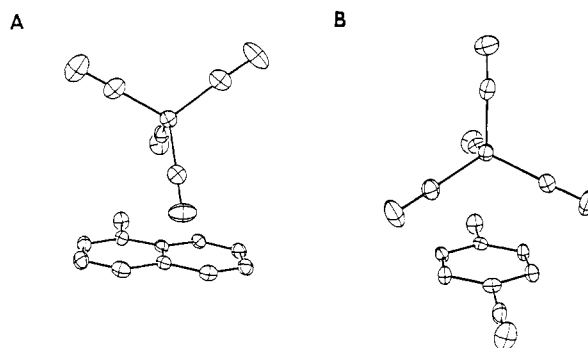


Figure 4. ORTEP diagram of (A) $\text{Q}^+\text{Co}(\text{CO})_4^-$ and (B) $\text{NCP}^+\text{Co}(\text{CO})_4^-$ locating the relevant charge-transfer interaction of the $\text{Co}(\text{CO})_4^-$ donor above the aromatic planes.

Table III. Solid-State and Solution IR Spectra of $\text{Co}(\text{CO})_4^-$ Salts^a

Cp_2Co^+	Q^+	NCP^+	Na^+	PPN^+
2007 (2006)	2007 (2004)	2006 (2003)	2025 (2007)	
1907 (1906)	1928 (1910)	1911 (1916)	1935 (1910) ^b	
1872 (1886)	1895 (1887)	1878 (1886)	1868 (1853) ^c	1883 (1887)
1858 (1870)		1865 (1870)		

^a ν_{CO} in cm^{-1} . Solid-state spectrum (10%) in KBr disk. Tetrahydrofuran solution (10^{-2} M) in parentheses. ^bResolved as two bands at 1899 and 1906 cm^{-1} in ref 46. ^cResolved as 1846 and 1856 cm^{-1} in ref 46; in addition to band at 1887 cm^{-1} .

Likewise, the molecular structures of the acceptor moieties Cp_2Co^+ and Q^+ existed as undistorted cations in the charge-transfer salts with respect to those found in other ionic salts.^{36,37} Most importantly, the X-ray crystallographic analyses of cobalticenium tetracarbonylcobaltate and iodide established the interionic separations of the Cp_2Co^+ /anion pairs³⁸ relevant to the charge-transfer absorptions in Table I. Thus the molecular (space-filling) models in Figure 3A and B illustrate the location of the anionic donors I^- and $\text{Co}(\text{CO})_4^-$ relative to the cobalticenium acceptor for optimal orbital overlap with the LUMO in the equatorial plane.³⁹ For the pyridinium salts of $\text{Co}(\text{CO})_4^-$, the analogous charge-transfer interaction of the tetracarbonylcobaltate donor placed it above the aromatic acceptor planes for optimal orbital overlap with the π -LUMOs of Q^+ and NCP^+ , as illustrated by the ORTEP diagrams in Figure 4. Such X-ray crystallographic structures indicated that these charge-transfer salts consisted of contact ion pairs (CIP) that were directionally constrained for optimum CT interaction in the crystal lattice.

III. Infrared Spectra of Charge-Transfer Salts as Contact Ion Pairs in the Solid State and in Solution.

The X-ray crystallographic

(34) (a) Klüfers, P. Z. *Kristallogr.* **1984**, *167*, 253. (b) Klüfers, P. Z. *Kristallogr.* **1983**, *165*, 217.

(35) Calderazzo, F.; Fachinetti, G.; Marchetti, F.; Zanazzi, P. F. *J. Chem. Soc., Chem. Commun.* **1981**, 181.

(36) Compare: Riley, P. E.; Davis, R. E. *J. Organomet. Chem.* **1978**, *152*, 209.

(37) Kobayashi, H.; Marumo, F.; Saito, Y. *Acta Crystallogr.* **1971**, *B27*, 373.

(38) The Co—Co distance of 6.88 Å in $\text{Cp}_2\text{Co}^+\text{Co}(\text{CO})_4^-$ compared with the Co—I separation of 4.75 Å in $\text{Cp}_2\text{Co}^+\text{I}^-$ (see Supplementary Material).

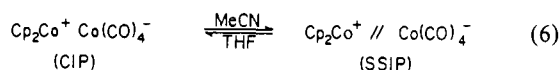
(39) For the shape of the LUMO in Cp_2Co^+ , see: Reference 40.

(40) Albright, T. A.; Burdett, J. K.; Whangbo, M. H. *Orbital Interactions in Chemistry*; Wiley: New York, 1985.

structures in Figures 3 and 4 emphasize the intimate contact that exists between the donor anion and the acceptor cation in charge-transfer salts. Such a close proximity of the anion/cation pairs was sufficient to distort the normally tetrahedral $\text{Co}(\text{CO})_4^-$ in Table II. The resulting decrease in symmetry could be readily detected by changes in the carbonyl bands in the infrared spectrum. For example, Table III includes the principal carbonyl bands (ν_{CO}) in the solid-state IR spectra of three charge-transfer salts, together with those of the Na^+ and PPN^+ salts for comparison. The single band at $\nu_{\text{CO}} = 1883 \text{ cm}^{-1}$ for the crystalline PPN^+ salt represented the T_2 mode of the undistorted tetrahedral $\text{Co}(\text{CO})_4^-$, in accord with the X-ray crystallographic structure of $\text{PPN}^+\text{Co}(\text{CO})_4^-$.⁴¹ In strong contrast, the IR spectra of the charge-transfer salts all showed the symmetry-forbidden A_1 band at $\sim 2005 \text{ cm}^{-1}$. Most importantly, the splitting of the major T_2 band in $\text{Q}^+\text{Co}(\text{CO})_4^-$ was akin to that previously observed in $\text{Na}^+\text{Co}(\text{CO})_4^-$ by Edgell and co-workers,¹⁹ and the IR spectra in Table III (entries 2 and 5) are both in accord with the expected three ($2A_1 + E$) bands for $\text{Co}(\text{CO})_4^-$ in C_{3v} symmetry established by X-ray crystallography.⁴² Moreover, the four carbonyl bands observed in the crystalline cobalticenium and cyanopyridinium analogues (entries 1 and 3) were consistent with the C_{2v} and C_s symmetry of $\text{Co}(\text{CO})_4^-$ in these salts, as established by X-ray crystallography (vide supra).^{43,44} In other words, the splittings of the carbonyl IR bands provided reliable and sensitive measures of the tetracarbonylcobaltate distortions that are extant in crystalline charge-transfer salts.

Having thus demonstrated the carbonyl IR bands as sensitive probes for $\text{Co}(\text{CO})_4^-$ in crystals, we now enquire whether they were applicable to the direct interaction of oppositely charged ions, which may persist as contact ion pairs (CIP) upon the dissolution of the charge-transfer salts.⁴⁵ Indeed, the comparison of the carbonyl IR bands in Table III shows that the charge-transfer salts dissolved in tetrahydrofuran were strikingly akin to those examined in the solid state. Furthermore, the difference between the ionic salts, $\text{Na}^+\text{Co}(\text{CO})_4^-$ and $\text{PPN}^+\text{Co}(\text{CO})_4^-$, was maintained in tetrahydrofuran solution. Since the latter derives from the undistorted $\text{Co}(\text{CO})_4^-$,⁴¹ we conclude that the structures of the crystalline charge-transfer salts, as established by X-ray crystallography (vide supra), were closely related to the contact ion pairs extant when these salts were dissolved in tetrahydrofuran.

It is important to emphasize that all of these salts, *regardless of the cation*, when dissolved in a polar solvent such as acetonitrile showed only a single band at $\nu_{\text{CO}} = 1892 \text{ cm}^{-1}$ in the carbonyl IR spectrum. Such a drastic simplification of the multiple splitting of the T_2 band of the charge-transfer salts with a simple change in solvent polarity was diagnostic of the return to a tetrahedral $\text{Co}(\text{CO})_4^-$, most likely as a solvent-separated ion pair (SSIP) previously observed with $\text{Na}^+\text{Co}(\text{CO})_4^-$ ⁴⁶ and $\text{Ti}^+\text{Co}(\text{CO})_4^-$ ¹⁴ and subsequently confirmed by conductivity measurements.^{44,47} Accordingly, we related the solvent-dependent changes in the carbonyl IR bands to the displacement of the contact ion pair (CIP), e.g.



where // denotes the solvent separation of the ion pair in which

(41) Chin, H. B.; Bau, R. *J. Am. Chem. Soc.* **1976**, *98*, 2434 (see footnote 11).

(42) Edgell, W. F.; Lyford, J.; Barbeta, A.; Jose, C. I. *J. Am. Chem. Soc.* **1971**, *93*, 6403.

(43) Braterman, P. S. *Metal Carbonyl Spectra*; Academic: New York, 1975.

(44) For other examples of distorted carbonylmetalates, see: (a) Pannell, K. H.; Jackson, D. *J. Am. Chem. Soc.* **1976**, *98*, 4443. (b) McVicker, G. B. *Inorg. Chem.* **1975**, *14*, 2087. (c) Darenbourg, M. Y.; Darenbourg, D. J.; Barros, H. L. C. *Inorg. Chem.* **1978**, *17*, 297. (d) Darenbourg, M. Y. *Prog. Inorg. Chem.* **1985**, *13*, 221.

(45) Free ions are unimportant in these nonaqueous media. See: Gordon, J. E. in ref 4, p 375ff.

(46) Edgell, W. F.; Hegde, S.; Barbeta, A. *J. Am. Chem. Soc.* **1978**, *100*, 1406.

(47) Darenbourg, M.; Barros, H.; Borman, C. *J. Am. Chem. Soc.* **1977**, *99*, 1647.

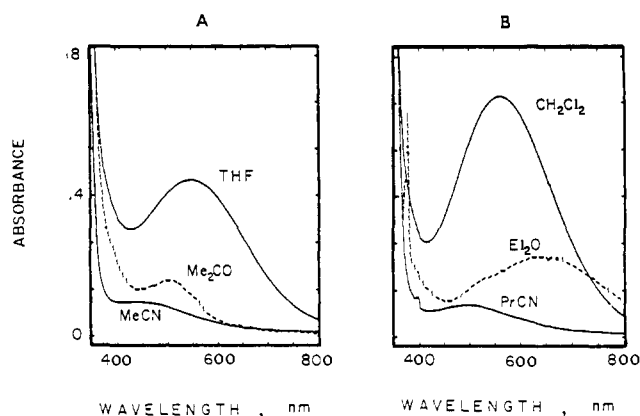


Figure 5. Solvent dependence of the charge-transfer spectrum of $\text{Q}^+\text{Co}(\text{CO})_4^-$ in solutions prepared from (A) THF (10^{-3} M), MeCN (10^{-2} M), and Me_2CO (10^{-3} M) and (B) CH_2Cl_2 (10^{-3} M), *n*-PrCN (10^{-3} M), and Et_2O (saturated).

Table IV. Solvatochromism of Charge-Transfer Salts^a

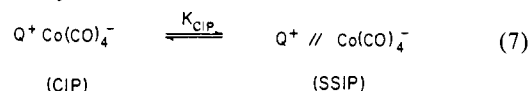
CT salt	THF	CH_2Cl_2	CHCl_3	Et_2O	MeCN ^b	BuCN
$\text{Q}^+\text{Co}(\text{CO})_4^-$	560	550	630	650	440	508
$\text{Q}^+\text{V}(\text{CO})_6^-$	630	670	758	760	518	516
$\text{PP}^+\text{Co}(\text{CO})_4^-$	492	480	522	556	430	454
$\text{Cp}_2\text{Co}^+\text{Co}(\text{CO})_4^-$	520	527	535	<i>d</i>	<i>c</i>	<i>c</i>
$\text{Cp}_2\text{Co}^+\text{V}(\text{CO})_6^-$	620	600	<i>d</i>	<i>d</i>	<i>c</i>	<i>c</i>
$\text{NCP}^+\text{V}(\text{CO})_6^-$	650	650	800	832	<i>c</i>	526
NCP^+I^-	<i>d</i>	444	456	<i>d</i>	400	420
ϵ^e	7.16	8.78	4.81	4.54	32.1	20.1
E_T^f	37.5	41.1	39.1	34.6	46.0	

^a Charge-transfer maximum (λ_{CT} , nm) in $1 \times 10^{-3} \text{ M}$ solutions at 25 °C, unless indicated otherwise. ^b At 10^{-2} M . ^c Unresolved shoulder obscured by low-energy tail absorption. ^d Insoluble salt. ^e From ref 48. ^f From ref 49.

$\text{Co}(\text{CO})_4^-$ was sufficiently unencumbered to adopt its most symmetric structure.

IV. Solvent Effects on the Charge-Transfer Salts. Solvatochromism. The marked change in the carbonyl IR bands accompanying the solvent variation from THF to MeCN coincided with the pronounced difference in color of the solutions. For example, the charge-transfer salt $\text{Q}^+\text{Co}(\text{CO})_4^-$ was intensely violet in THF but imperceptibly orange in MeCN at the same concentration. The quantitative effects of such a solvatochromism are illustrated in Figure 5 by (a) the shifts of the absorption maximums and (b) the diminution in the absorbances at λ_{CT} . The concomitant bathochromic shift and hyperchromic increase in the charge-transfer bands in Figure 5A followed the sizable decrease in solvent polarity from acetonitrile to tetrahydrofuran as evaluated by the dielectric constants $\epsilon = 37.5$ and 7.6, respectively.^{48,49} The same but even more pronounced trend was apparent (Figure 5B) in passing from butyronitrile to dichloromethane to diethyl ether with $\epsilon = 26$, 9.1, and 4.3, respectively.

The marked variation in λ_{CT} with solvent polarity (Table IV) paralleled the behavior of the carbonyl IR bands (vide supra), and the solvatochromism was thus readily ascribed to the same displacement of the CIP (eq 6) and its associated charge-transfer band. As such, the reversible equilibrium between CIP and SSIP was described by



where the dissociation constant K_{CIP} applied to a particular solvent and temperature. The quantitative effects of solvent polarity on the dissociation constant were evaluated spectrophotometrically

(48) Dean, J. A., Ed. *Lange's Handbook of Chemistry*, 12th ed.; McGraw Hill: 1979.

(49) For the related E_T values, see: Reichardt, C. *Solvent Effects in Organic Chemistry*; Verlag Chemie: New York, 1979.

Table V. CIP Dissociation of Charge-Transfer Salts in Polar and Nonpolar Solvents^a

CT salt	solvent	λ_{mon}^b , nm	K_{CIP} , M	ϵ_{CT} , M ⁻¹ cm ⁻¹
Cp ₂ Co ⁺ Co(CO) ₄ ⁻	MeCN	520	1.1 × 10 ⁻²	180
	CH ₂ Cl ₂	520	1.5 × 10 ⁻⁴	230
Q ⁺ Co(CO) ₄ ⁻	MeCN	458	8.1 × 10 ⁻²	227
	THF	550	1.2 × 10 ⁻⁴	420
	CH ₂ Cl ₂	560	1.5 × 10 ⁻⁵	590
PP ⁺ Co(CO) ₄ ⁻	CH ₂ Cl ₂	494	2.3 × 10 ⁻⁵	380
PPN ⁺ Co(CO) ₄ ⁻	THF ^c		9.4 × 10 ⁻⁵	
PPN ⁺ V(CO) ₆ ⁻	THF ^c		1.2 × 10 ⁻⁴	
PPN ⁺ BPh ₄ ⁻	THF ^c		9.1 × 10 ⁻⁵	

^a At 25 °C in the concentration range of 10⁻⁴–10⁻¹ M. ^b Monitoring wavelength for CT band. ^c From ref 47.

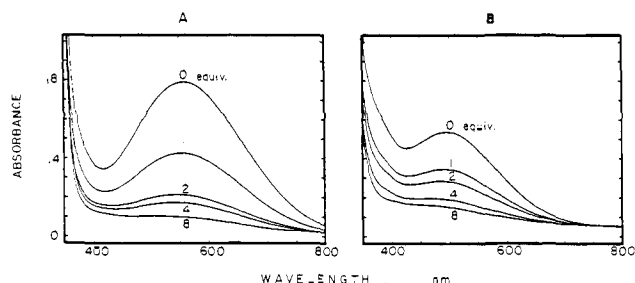


Figure 6. Salt effect on the charge-transfer spectra of (A) 1.5 × 10⁻³ M Q⁺Co(CO)₄⁻ and (B) 1.0 × 10⁻³ M PP⁺Co(CO)₄⁻ in CH₂Cl₂ containing 0, 1, 2, 4, and 8 equiv of TBAP.

by measuring the change in the CT absorbance A_{CT} at various concentrations C of the charge-transfer salt from the relationship^{50,51}

$$K_{\text{CIP}} = \frac{A_{\text{CT}}}{\epsilon_{\text{CT}}} + \frac{C^2 \epsilon_{\text{CT}}}{A_{\text{CT}}} - 2C \quad (8)$$

The CIP dissociation constants evaluated according to eq 8 (see Experimental Section) are listed in Table V for some typical charge-transfer salts in both polar and nonpolar solvents. The values of K_{CIP} measured conductometrically⁴⁷ for the related ionic salts, PPN⁺Co(CO)₄⁻, PPN⁺V(CO)₆⁻, and Na⁺BPh₄⁻, are included in the table for comparison. Two features in Table V are particularly noteworthy. First, the magnitudes of K_{CIP} in the nonpolar solvents (THF and CH₂Cl₂) were at least 100-fold smaller than those in the polar MeCN. Thus, at the concentrations employed in the IR studies (Table III), the charge-transfer salts existed in THF primarily (>90%) as the contact ion pair. Second, extinction coefficient ϵ_{CT} evaluated at the maximum of the charge-transfer band λ_{CT} was relatively invariant with solvent polarity.⁵² This suggested that the same (or closely related)⁵³ CIPs were always formed, and the effect of solvent polarity largely resided with changes in K_{CIP} . Such a solvent effect on the thermodynamics of CIP dissociation was indeed consistent with the influence of added salts (vide infra, Figure 7).

V. Salt Effects on the Charge-Transfer Salts in Solution. The addition of small amounts of inert salts such as tetrabutylammonium perchlorate (TBAP) or hexafluorophosphate (TBAH) to solutions of charge-transfer salts induced large changes in the intensity of the charge-transfer absorption bands. The magnitude of the salt effect was most pronounced in nonpolar solvents (THF, CH₂Cl₂), as illustrated in Figure 6. The monotonic decrease in the CT absorbance with increasing amounts of added TBAP was

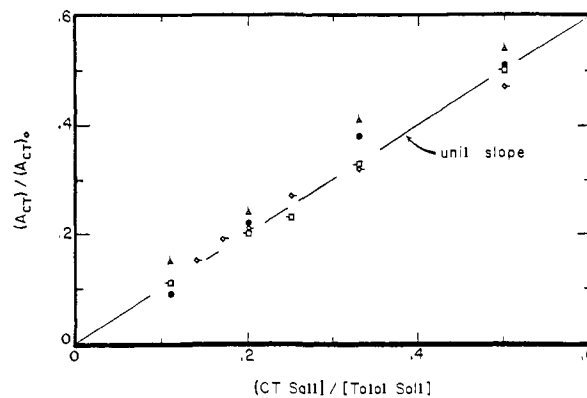
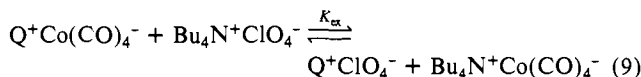


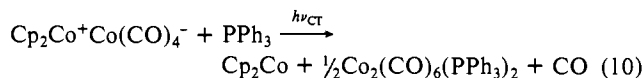
Figure 7. Ion-pair exchange of the charge-transfer salts Cp₂Co⁺Co(CO)₄⁻ (□), Q⁺Co(CO)₄⁻ (●), (C₆H₆)₂Cr⁺Co(CO)₄⁻ (▲), and PP⁺Co(CO)₄⁻ (◇) in 2 × 10⁻³ M CH₂Cl₂ containing 2–20 mM TBAP.

characteristic of the facile competition for the contact ion pair, i.e.⁵⁴

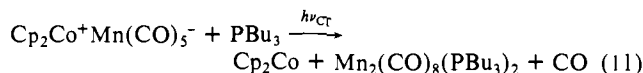


Indeed, the single linear relationship between the charge-transfer absorbance and the mole fraction of the inert salt (TBAP) added to Cp₂Co⁺Co(CO)₄⁻, PP⁺Co(CO)₄⁻, Q⁺Co(CO)₄⁻, and (C₆H₆)₂Cr⁺Co(CO)₄⁻ with the line in Figure 7 drawn with unit slope indicated that $K_{\text{ex}} = 1.0$ (see Experimental Section). Such a magnitude of K_{ex} pointed to the nonspecific interchange between contact ion pairs that effectively served to disassemble the intimate charge-transfer ion pair Q⁺Co(CO)₄⁻, without recourse to solvent variation as inSSIP formation (vide supra). As such, we envisage the primary salt effect in eq 9 to be largely governed by ion-pair electrostatics. This situation is to be contrasted with the effect of salt on the charge-transfer absorption of Ti⁺Co(CO)₄⁻.¹⁴

VI. Photoexcitation of Charge-Transfer Salts in Solution. The red-brown solution of the contact ion pair Cp₂Co⁺Co(CO)₄⁻ in dichloromethane showed no change, even upon prolonged irradiation (8 h) of the charge-transfer band at $\lambda > 520$ nm. However, the repetition of the experiment in the presence of triphenylphosphine led to the spontaneous evolution of carbon monoxide and the disappearance of Co(CO)₄⁻, as judged by the diminution of its characteristic carbonyl IR band at $\nu_{\text{CO}} = 1887$ cm⁻¹. In its place a new band appeared at $\nu_{\text{CO}} = 1958$ cm⁻¹ for the dimeric Co₂(CO)₆(PPh₃)₂⁵⁵ that was isolated in 65% yield together with cobaltocene according to the stoichiometry



Cobaltocene and the analogous cobalt dimer Co₂(CO)₆(PMe₂Ph)₂ were also obtained when triphenylphosphine was replaced with dimethylphenylphosphine, as shown in Table VI. The stoichiometry in eq 10 corresponded formally to an oxidation-reduction process, in which the 1-electron reduction of Cp₂Co⁺ to cobaltocene was accompanied by the 1-electron oxidation of Co(CO)₄⁻ to the carbonylcobalt(0) dimer. Moreover, the analogous photoredox dimerization of the corresponding carbonylmanganate salt occurred only when tri-*n*-butylphosphine was present, i.e.



Since these photoredox processes were specifically promoted by the CT excitation of the contact ion pair (CIP), they will be referred to hereafter as *charge-transfer dimerizations*.

(50) Drago, R. S.; Rose, N. J. *J. Am. Chem. Soc.* **1959**, *81*, 6138.

(51) Note that this measurement makes no distinction betweenSSIP and free ions, or of ion triplets, etc. See, e.g.: Wang, H. C.; Levin, G.; Szwarc, M. *J. Am. Chem. Soc.* **1978**, *100*, 6137.

(52) For the slight variations in λ_{CT} with solvent polarity, see: Davis, K. M. C. *Molecular Association*; Foster, R., Ed.; Academic: New York, 1975; Vol. 1, p 151ff.

(53) Conceivably, with slightly different interionic separations ($r_{\text{A}^+\text{D}^-}$).

(54) See: Masnovi, J. M.; Kochi, J. K. *J. Am. Chem. Soc.* **1985**, *107*, 7880.

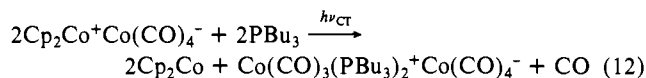
(55) Manning, A. R. *J. Chem. Soc. A* **1968**, 1135.

Table VI. Charge-Transfer Photochemistry of Contact Ion Pairs^a

CT salt (10 ² M)		added L (10 ² M)		products ^b (%)	
Cp ₂ Co ⁺ Co(CO) ₄ ⁻	(3.8) ^c	PPh ₃	(4.0)	Co ₂ (CO) ₆ L ₂	(65) ^d
	(0.34)	PMe ₂ Ph	(0.8)	Co ₂ (CO) ₆ L ₂	(50)
	(1.0)	P(OPh) ₃	(1.0)	Cp ₂ Co ⁺ Co(CO) ₃ L ⁻	(62)
	(1.0)	PBu ₃	(1.5)	Co ₂ (CO) ₆ L ₂	(15)
Q ⁺ Co(CO) ₄ ⁻	(1.2) ^c	PPh ₃	(2.4)	Co(CO) ₃ L ₂ ⁺ Co(CO) ₄ ⁻	(60)
	(1.4)	PMe ₂ Ph	(2.0)	Co ₂ (CO) ₆ L ₂	(88) ^d
	(1.0)	PBu ₃	(1.2)	Co(CO) ₃ L ₂ ⁺ Co(CO) ₄ ⁻	(90)
	(0.30)	P(OPh) ₃	(0.60)	Co(CO) ₃ L ₂ ⁺ Co(CO) ₄ ⁻	(95) ^e
	(0.8)	PBu ₃	(2.4)	Co ₂ (CO) ₆ L ₂	(80)
PP ⁺ Co(CO) ₄ ⁻ (C ₆ H ₆) ₂ Cr ⁺ Co(CO) ₄ ⁻	(0.8)	PBu ₃	(2.4)	Co ₂ (CO) ₆ L ₂	(22) ^f
	(0.8)	PMe ₂ Ph	(1.8)	Co(CO) ₃ L ₂ ⁺ Co(CO) ₄ ⁻	(16) ^g
Cp ₂ Co ⁺ Mn(CO) ₅ ⁻	(1.0)	PBu ₃	(2.0)	Co(CO) ₃ L ₂ ⁺ Co(CO) ₄ ⁻	(18) ^g
	(1.2) ^j	PBu ₃	(7.0)	Mn ₂ (CO) ₈ L ₂	(16) ^h
Cp ₂ Co ⁺ V(CO) ₆ ⁻	(1.2)	PPh ₃	(7.0)	i	
	(0.4)	PMe ₃	(0.7)	i	
	(1.0)	PPh ₃	(2.0)	i	

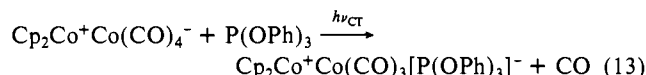
^aIrradiation with $\lambda > 550$ nm for ~ 2 h in THF at 25 °C, unless indicated otherwise. ^bProducts by quantitative IR analysis of carbonyl bands (see Experimental Section), except where noted. ^cCH₂Cl₂ with $\lambda > 520$ nm. ^dIsolated. ^eIsolated 75%. ^fMaximum yield at 50% conversion. ^gMaximum yield at $\sim 30\%$ conversion. ^hStationary-state yield. ⁱNo products observed after 7-h irradiation. ^jAcetone.

When the most basic phosphine *n*-Bu₃P was used as the additive in the charge-transfer photochemistry of the contact ion pair Cp₂Co⁺Co(CO)₄⁻, it again led to CO evolution and cobaltocene was isolated in 41% yield by sublimation from the reaction mixture. However a different carbonyl product was formed in 60% yield according to the stoichiometry



together with smaller amounts of the dimeric Co₂(CO)₆(PBu₃)₂ reminiscent of the stoichiometry in eq 10, as shown in Table VI (entry 3). The photoinduced process in eq 12 (like that in eq 10) formally represented an oxidation-reduction of the charge-transfer salt. Accordingly, this photochemical process will be referred to hereafter simply as *charge-transfer disproportionation*.

The photoinduced reaction of the contact ion pair Cp₂Co⁺Co(CO)₄⁻ took a third course in Table VI (entry 4) when either the triphenylphosphine or tributylphosphine additive was replaced with triphenylphosphite, viz.



which corresponded to an overall substitution of Co(CO)₄⁻ by a single P(OPh)₃ ligand. Control experiments established that (a) neither PPh₃, PBu₃, nor P(OPh)₃ had any effect on the charge-transfer spectrum of Cp₂Co⁺Co(CO)₄⁻ in Figure 1B and (b) no thermal reaction occurred in the absence of light. In order to differentiate the photoinduced process in eq 13 from that in either eq 10 or 12, it will be simply referred to hereafter as *charge-transfer substitution*.

The photochemical behavior of the other charge-transfer salts in Table I was comparable to that of Cp₂Co⁺Co(CO)₄⁻. Thus the orange, purple, and green solutions of PP⁺Co(CO)₄⁻, Q⁺Co(CO)₄⁻, and (C₆H₆)₂Cr⁺Co(CO)₄⁻, respectively, in dichloromethane were stable to visible radiation (with $\lambda > 550$ nm) for prolonged periods. Similarly the carbonylvanadate and manganese salts Cp₂Co⁺V(CO)₆⁻ and Cp₂Co⁺Mn(CO)₅⁻ were unaffected by visible radiation with $\lambda > 520$ nm. However, owing to the generally inert character of these charge-transfer salts, all further CT photochemical studies focused on the carbonylcobaltate salts. In each case, the actinic radiation of the charge-transfer salts in dichloromethane or tetrahydrofuran containing added ligand L = phosphine or phosphite resulted in the liberation of 1 mol of carbon monoxide. The stoichiometry leading to either CT dimerization, disproportionation, or substitution as given in eq 10, 12, and 13, respectively, varied with the additive L. Isolation of the carbonylmetal products in Table VI and IR spectral analyses based on the characteristic carbonyl bands (Experimental Section)

Table VII. Quantum Yield for Charge-Transfer Disproportionation and Substitution of Co(CO)₄⁻ Contact Ion Pairs^a

CT salt (10 ³ M)	PBu ₃ , 10 ² M	conv. ^b %	Φ _p ^c	
Q ⁺ Co(CO) ₄ ⁻	(9.0)	1.8	10	0.08
	(8.8)	3.5	9	0.19
	(9.5)	7.6	25	0.35
	(9.9)	11	19	0.44
	(9.7)	17	15	0.42
Cp ₂ Co ⁺ Co(CO) ₄ ⁻	(9.5)	24	18	0.40 ^d
	(14)	3.9	9	0.06
	(13)	11	4	0.11
(C ₆ H ₆) ₂ Cr ⁺ Co(CO) ₄ ⁻	(13)	24	10	0.14
	(14)	2.5	10	0.10
	(12)	6.6	14	0.55
	(17)	10	28	0.76
	(15)	22	18	0.69
Cp ₂ Co ⁺ Mn(CO) ₅ ⁻	(24) ^e	6.0	1.5	<0.05 ^f
Cp ₂ Co ⁺ V(CO) ₆ ⁻	(4.0)	7.0	g	<0.001

^aIrradiation at 550 ± 10 nm in THF at 25 °C, unless indicated otherwise. ^bConversion assuming half of Co(CO)₄⁻ available. ^cProduction of Co(CO)₃[PBu₃]₂⁺ unless indicated otherwise. ^dTransmission correction of 10%. ^eAcetone. ^fFor Mn₂(CO)₈[PBu₃]₂. ^gNot detected.

indicated that one of the three processes was usually dominant for certain cationic acceptors with different phosphines (or phosphites).

At this juncture, it is important to emphasize that the photoinduced dimerization, disproportionation, and substitution always arose directly from the charge-transfer excitation of only the contact ion pair. Thus, the use of visible light with $\lambda > 520$ nm as the radiation source ensured the excitation of only the charge-transfer absorption bands in Figure 1. Since these CT absorptions related specifically to the contact ion pair (see Table V), there was no ambiguity about the adventitious local excitation of either the separate anion or cation, or the photochemical generation of intermediates that did not arise from the CT excitation of the contact ion pair.

VII. Quantum Yields for the Charge-Transfer Photochemistry of Contact Ion Pairs. Owing to the critical role of the additive L on the charge-transfer photochemistry of contact ion pairs in Table VI, it was important to establish quantitatively the dependence of the quantum yield Φ on phosphine concentration. The charge-transfer disproportionation of Cp₂Co⁺Co(CO)₄⁻, Q⁺Co(CO)₄⁻, and (C₆H₆)₂Cr⁺Co(CO)₄⁻ with L = tri-*n*-butylphosphine was chosen for quantum yield measurements since only a single, pale yellow salt Co(CO)₃L₂⁺Co(CO)₄⁻ was formed (Table VI). Most importantly, the weak visible absorbance of Co(CO)₃L₂⁺Co(CO)₄⁻ at $\lambda > 500$ nm caused no important interference of the CT excitation for the contact ion pairs. The quantum yields in

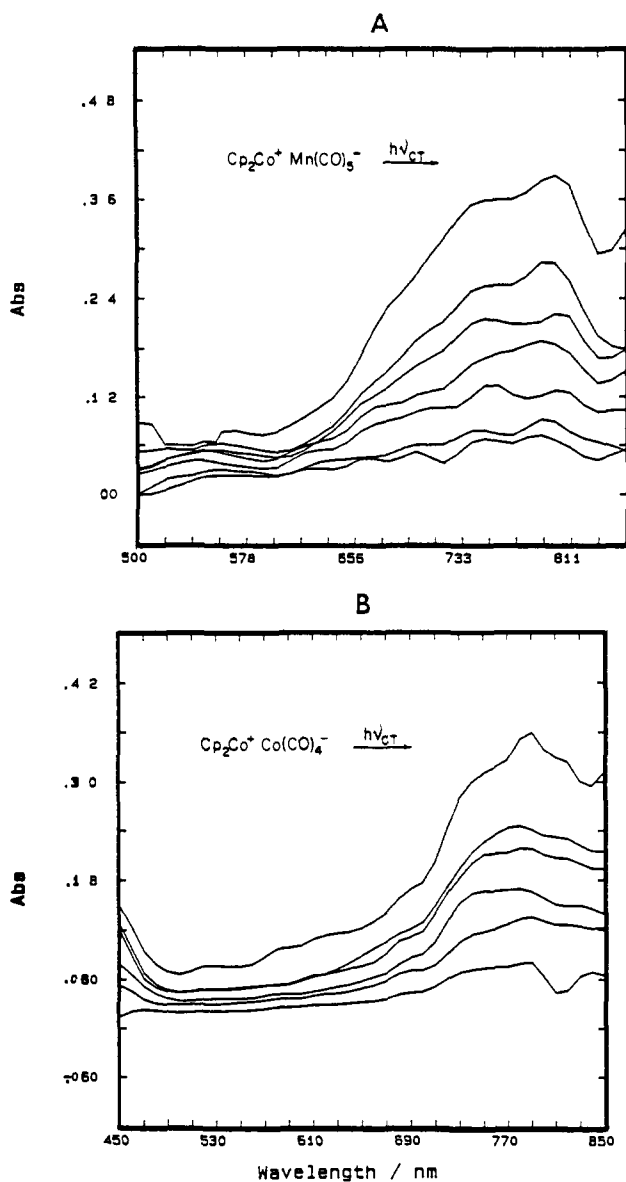


Figure 8. Time-resolved difference spectra resulting from the 532-nm excitation of (A) 1.4×10^{-2} M $\text{Cp}_2\text{Co}^+\text{Mn}(\text{CO})_5^-$ at 0.9, 1.4, 1.8, 2.3, 2.8, 3.7, and 4.7 μs and (B) 1.3×10^{-2} M $\text{Cp}_2\text{Co}^+\text{Co}(\text{CO})_4^-$ at 16, 20, 25, 28, 38, and 54 μs in Me_2CO .

Table VII were based on Reineckate actinometry using monochromatic light ($\lambda = 550 \pm 10$ nm)⁵⁶ and carried out by quantitative IR analysis of the characteristic carbonyl bands of the cationic moiety $\text{Co}(\text{CO})_3\text{L}_2^+$, as described in the Experimental Section. For each of the charge-transfer salts, the value of Φ_p reached a limiting value, which decreased in the order $(\text{C}_6\text{H}_6)_2\text{Cr}^+ > \text{Q}^+ > \text{Cp}_2\text{Co}^+$ for charge-transfer disproportionation (see eq 12). The quantum yields for charge-transfer dimerization (eq 10) and substitution (eq 13) could not be measured reliably owing to the spectral interference by the products $\text{Co}_2(\text{CO})_6\text{L}_2$ and $\text{Co}(\text{CO})_3\text{L}^-$ that arose from their intense absorption bands which tailed into the visible region.^{57,58} However we qualitatively judge from the product conversions in Table VI that the photoefficiencies of charge-transfer dimerization and substitution were not widely divergent from the quantum yields measured in Table VII.

VIII. Time-Resolved Spectra of Reactive Intermediates in the Charge-Transfer Photochemistry of Contact Ion Pairs. In order

(56) Wegner, E. E.; Adamson, A. W. *J. Am. Chem. Soc.* **1966**, *88*, 394.

(57) (a) Geoffroy, G. L.; Wrighton, M. S. *Organometallic Photochemistry*; Academic: New York, 1979. (b) Meyer, T. J.; Caspar, J. V. *Chem. Rev.* **1985**, *85*, 187.

(58) Lee, K. Y.; Kochi, J. K. *Inorg. Chem.* **1989**, *28*, 567.

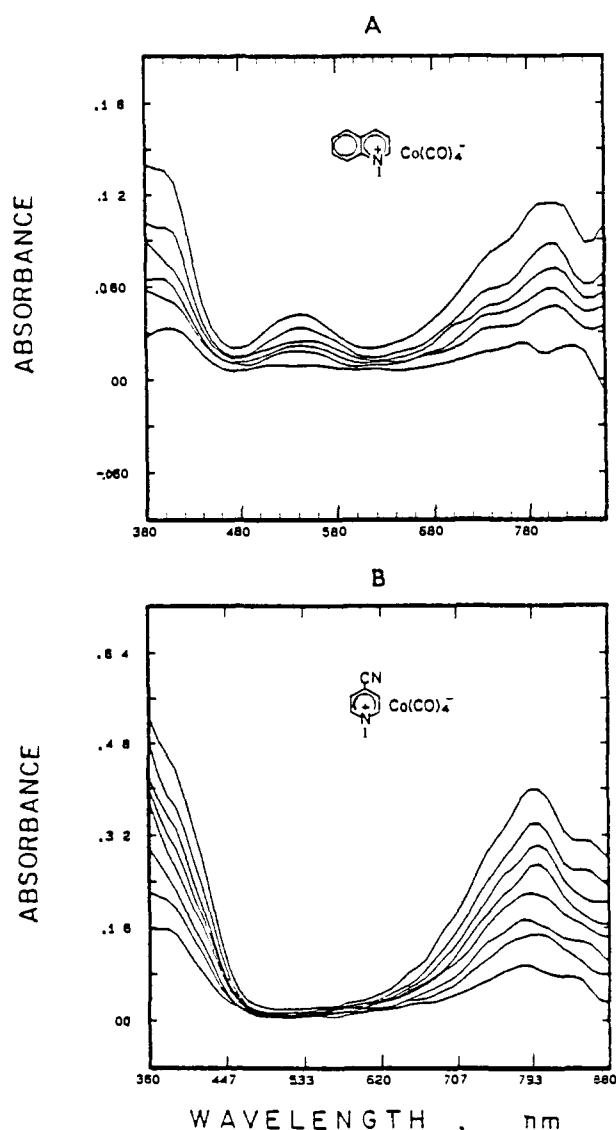


Figure 9. Transient absorption spectra (difference) from the 532-nm excitation of (A) 1.0×10^{-2} M $\text{Q}^+\text{Co}(\text{CO})_4^-$ at 60, 83, 106, 128, 150, and 217 μs and (B) 1.5×10^{-2} M $\text{NCP}^+\text{Co}(\text{CO})_4^-$ at 16, 21, 25, 29, 33, 46, 58, and 72 μs in Me_2CO .

to identify the reactive intermediates in the charge-transfer photochemistry of the contact ion pairs, we examined the time-resolved spectra immediately following the application of a 10-ns pulse consisting of the second harmonic at 532 nm of a Q-switched Nd^{3+} -YAG laser. The wavelength of this radiation source was ideally suited for the specific excitation of the contact ion pairs (see Table V). Accordingly, the time-resolved spectra in Figure 8 obtained from $\text{Cp}_2\text{Co}^+\text{Mn}(\text{CO})_5^-$ and $\text{Cp}_2\text{Co}^+\text{Co}(\text{CO})_4^-$ related directly to the charge-transfer photochemistry in Table VI.

Most notably, the intense band centered at $\lambda_{\text{max}} = 800$ nm in Figure 8A was identical with the 17-electron radical $\text{Mn}(\text{CO})_5^*$ that was previously generated from the direct homolytic cleavage of the dimeric $\text{Mn}_2(\text{CO})_{10}$.⁵⁹ Other flash photolytic studies,⁶⁰ as well as pulse radiolysis⁶¹ and matrix isolation,⁶² have verified

(59) Rothberg, L. J.; Cooper, N. J.; Peters, K. S.; Vaida, V. *J. Am. Chem. Soc.* **1982**, *104*, 3536.

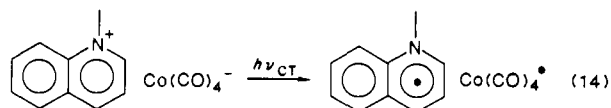
(60) Walker, H. W.; Herrick, R. S.; Olsen, R. J.; Brown, T. L. *Inorg. Chem.* **1984**, *23*, 3748.

(61) Waltz, W. L.; Hackelberg, O.; Dorfman, L. M.; Wojcicki, A. *J. Am. Chem. Soc.* **1978**, *100*, 7259.

(62) (a) Church, S. P.; Poliakov, M.; Timney, J. A.; Turner, J. J. *J. Am. Chem. Soc.* **1981**, *103*, 7515. (b) A variety of other 17-electron carbonylmetal radicals commonly show low-energy absorptions in the spectral region $\lambda \sim 600$ –800 nm. See: Baird, M. C. *Chem. Rev.* **1988**, *88*, 1217, and references therein.

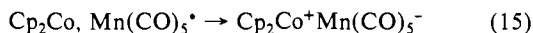
the spectral assignment of $\text{Mn}(\text{CO})_5^*$ with $\lambda_{\text{max}} \sim 800$ nm.

The analogous observation of the spectral transient absorbing at $\lambda_{\text{max}} = 780$ nm from the CT excitation of $\text{Cp}_2\text{Co}^+\text{Co}(\text{CO})_4^-$ could be similarly ascribed to the 17-electron radical $\text{Co}(\text{CO})_4^*$ in Figure 8B. Unfortunately, the absorption spectrum of this carbonylcobalt(0) radical was not available for verification from other studies.⁶³ However, if one considers the location of absorption bands of their anionic precursors $\text{Co}(\text{CO})_4^-$ and $\text{Mn}(\text{C}-\text{O})_5^-$ at $\lambda_{\text{max}} = 320$ and 330 nm, respectively, it may not be unreasonable to expect a similar relationship for the isoelectronic radicals $\text{Co}(\text{CO})_4^*$ and $\text{Mn}(\text{CO})_5^*$ in Figure 8. Be that as it may, the laser-pulse excitation of the quinolinium and cyanopyridinium salts of $\text{Co}(\text{CO})_4^-$ produced the same spectral transient with $\lambda_{\text{max}} = 780$ nm, as shown in Figure 9. Most revealingly, the simultaneous appearance of two bands at $\lambda_{\text{max}} = 550$ and ~ 380 nm (end absorption) from the CT excitation of $\text{Q}^+\text{Co}(\text{CO})_4^-$ in Figure 9A could be readily assigned to the quinolinyl radical (Q^*) that was independently generated earlier.⁶⁴ Moreover, the high-energy tail absorption in Figure 9B obtained from the CT excitation of $\text{NCP}^+\text{Co}(\text{CO})_4^-$ was in accord with the known cyanopyridinyl radical (NCP^*) with its intense absorption at $\lambda_{\text{max}} = 390$ nm.⁶⁵ Taken together, the time-resolved spectra in Figures 8B and 9 provide strong support for the primary step in the photoactivation of tetracarbonylcobaltate salts, e.g.



that is wholly consistent with the photoredox process for the pentacarbonylmanganate salt (vide supra). These time-resolved spectroscopic studies have thus shown that the charge-transfer excitation of CIPs resulted in simultaneous production of the reactive 17-electron carbonylmetal radicals [$\text{Mn}(\text{CO})_5^*$, $\text{Co}(\text{CO})_4^*$, etc.] together with the reduced acceptor radical (Cp_2Co , Q^* , NCP^* , etc.). Furthermore the time scale of the CT photoexcitation indicates that these radicals are initially paired within the solvent cage.⁶⁶

IX. Temporal Evolution of Transient Radical Pairs from the Charge-Transfer Excitation of CIPs. The absence of productive photochemistry upon the steady-state irradiation of contact ion pairs alone in solution (i.e., without added phosphine) was consistent with the spontaneous return of the transient radicals to the ground state intact, e.g.



Such a regeneration of the CIP from the radical pair accorded with the invariance of the charge-transfer spectra even upon prolonged irradiation. Back electron transfer from the radical pair was also supported in the time-resolved spectroscopic studies by the restoration of the transient absorbances to the original base lines in Figures 8 and 9.

Kinetics for the return of the radical pair from $\text{Cp}_2\text{Co}^+\text{Mn}(\text{CO})_5^-$ were measured by following the absorbance change of $\text{Mn}(\text{CO})_5^*$ at the monitoring wavelength of $\lambda_{\text{mon}} = 800$ nm. Figure 10A illustrates a typical decay curve for $\text{Mn}(\text{CO})_5^*$ following the CT excitation at 532 nm of $\text{Cp}_2\text{Co}^+\text{Mn}(\text{CO})_5^-$ in Me_2CO with the 10-ns laser pulse. The reaction order of the kinetics was established by linear least-squares computer fits of the observed decrease of the absorbance with time, as detailed in the Exper-

(63) The spectral observation of $\text{Co}(\text{CO})_4^*$ was unfortunately not extended beyond $\lambda = 700$ nm by: (a) Hanlan, L. A.; Huber, H.; Kundig, E. P.; McGarvey, B. R.; Ozin, G. A. *J. Am. Chem. Soc.* **1975**, *97*, 7054. (b) For the complex photochemistry of $\text{Co}_2(\text{CO})_8$, see: Wegman, R. W.; Brown, T. L. *Inorg. Chem.* **1983**, *22*, 183.

(64) (a) Cozzens, R. F.; Gover, T. A. *J. Phys. Chem.* **1970**, *74*, 3003. In this study, the high-energy band of Q^* at ~ 400 nm was obscured by the very strong absorption by I_2^- . (b) In our study, the observation of the maximum of the high-energy band was complicated by tail absorptions of $\text{Mn}(\text{CO})_5^*$ and $\text{Co}(\text{CO})_4^*$.

(65) Itoh, M.; Nagakura, S. *Bull. Chem. Soc. Jpn.* **1966**, *39*, 369.

(66) Compare: Hilinski, E. F.; Masnovi, J. M.; Kochi, J. K.; Rentzepis, P. M. *J. Am. Chem. Soc.* **1984**, *106*, 8071.

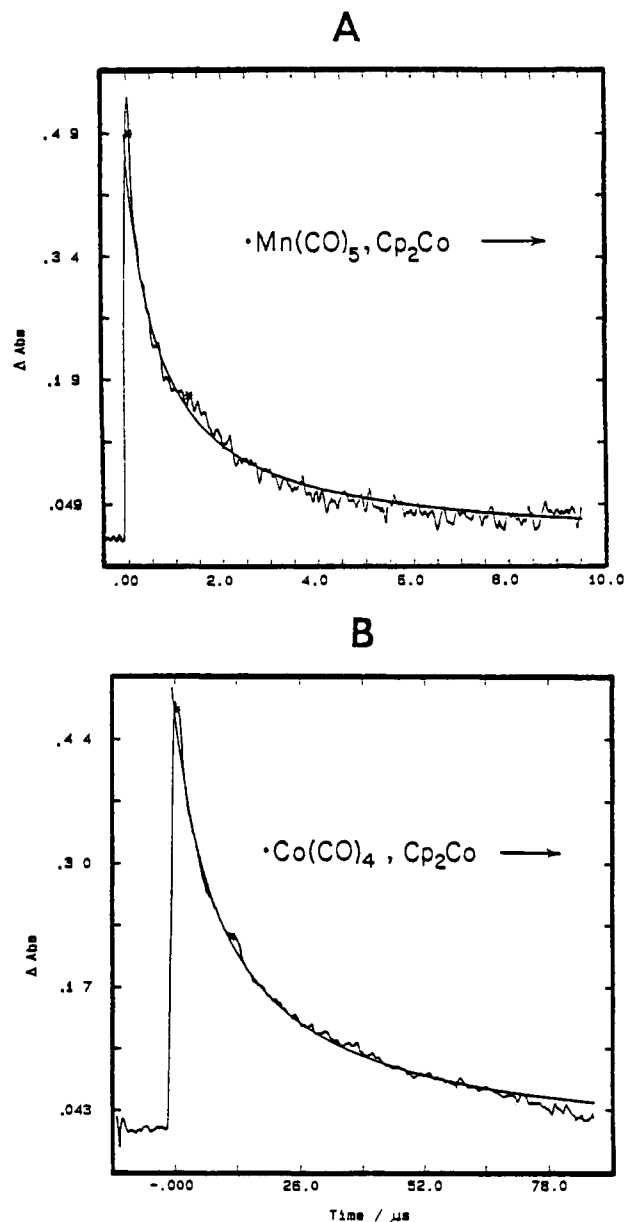
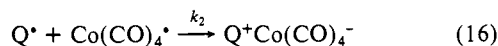


Figure 10. Decay of the CT transients from (A) 2.0×10^{-2} M $\text{Cp}_2\text{Co}^+\text{Mn}(\text{CO})_5^-$ and (B) 1.0×10^{-2} M $\text{Cp}_2\text{Co}^+\text{Co}(\text{CO})_4^-$ in Me_2CO at 25°C by following the absorbance change at $\lambda_{\text{mon}} = 800$ and 780 nm, respectively.

imental Section. Thus the second-order kinetics for the disappearance of $\text{Mn}(\text{CO})_5^*$ was demonstrated by the excellent fit of the smooth computed curve to the experimental decay in Figure 10A. The second-order rate constant k_2 evaluated in this manner was insensitive to solvent variation (Table VIII, entries 1 and 2).

Disappearance of the radicals derived from such carbonylcobaltate salts as $\text{Cp}_2\text{Co}^+\text{Co}(\text{CO})_4^-$ also followed the same second-order kinetics (Figure 10B). It is noteworthy that the CT excitation of the quinolinium salt $\text{Q}^+\text{Co}(\text{CO})_4^-$ allowed a pair of second-order rate constants to be extracted from the absorbance decays at $\lambda_{\text{mon}} = 550$ and 780 nm (Table VIII, entry 4). Assignment of the latter to the 17-electron $\text{Co}(\text{CO})_4^*$ (vide supra) then defined the second-order kinetics to derive from the mutual annihilation of the radicals, i.e.,



Furthermore, the same kinetic relationship held for the pair of radicals from the cyanopyridinium salt $\text{NCP}^+\text{Co}(\text{CO})_4^-$ in Table VIII (entry 7). Since the absorbance at $\lambda_{\text{mon}} = 380$ nm did not return completely to the base line, it is possible that the highly

Table VIII. Kinetics for the Radical-Pair Return to the Contact Ion Pair^a

contact ion pair (10 ³ M)		solvent	radical	nm ^b	τ , ^c μ s	k , ^d $\text{A}^{-1} \text{s}^{-1}$
Cp ₂ Co ⁺ Mn(CO) ₅ ⁻	(10)	MeCN	Mn(CO) ₅ [*]	[790]	0.4	2.7 × 10 ⁷
Cp ₂ Co ⁺ Mn(CO) ₅ ⁻	(20) ^e	Me ₂ CO	Mn(CO) ₅ [*]	[790]	0.3	4.4 × 10 ⁷
Cp ₂ Co ⁺ Co(CO) ₄ ⁻	(13)	Me ₂ CO	Co(CO) ₄ [*]	[780]	10	2.0 × 10 ⁶
Q ⁺ Co(CO) ₄ ⁻	(8)	Me ₂ CO	Co(CO) ₄ [*]	[780]	8	1.6 × 10 ⁷
			Q [*]	[550]	6	0.9 × 10 ⁷
Q ⁺ Co(CO) ₄ ⁻	(0.6)	CH ₂ Cl ₂	Q [*]	[550]	14	1.4 × 10 ⁷
Q ⁺ Co(CO) ₄ ⁻ /PBu ₃	<i>f</i>	CH ₂ Cl ₂	Q [*]	[550]	17	3.7 × 10 ⁶
NCP ⁺ Co(CO) ₄ ⁻	(11)	Me ₂ CO	Co(CO) ₄ [*]	[780]	21	1 × 10 ⁶
			NCP [*]	[380]	42	5 × 10 ⁵

^a As charge-transfer salt dissolved in 3 mL of solvent at 25 °C and irradiation at 532 nm, unless indicated otherwise. ^b λ_{max} . ^c Apparent half-life. ^d Second-order rate constant in absorbance units, reliability $\pm 20\%$. ^e From an equimolar mixture of PPN⁺Mn(CO)₅⁻ and Cp₂Co⁺PF₆⁻. ^f Q⁺Co(CO)₄⁻ (1.55 mM) plus added PBu₃ (10 mM).

persistent NCP⁺⁶⁷ did not always undergo mutual annihilation as presented in eq 16. The kinetic results in Table VIII also showed that radical decay suffered only a minor retardation in the presence of added phosphine (entry 6).

Discussion

The well-defined 1:1 salts from anionic (carbonylmetalate) donors and cationic (metallocenium and pyridinium) acceptors in Table I exhibit ideal properties for photochemical and photo-physical studies of charge-transfer excitation within contact ion pairs.

I. Structures of Contact Ion Pairs (CIP) in Solution from X-ray Crystallography. The X-ray crystallographic structures shown in Figures 3 and 4 delineate (a) the interionic separations, (b) the spatial cation/anion orientations, and (c) the deviations from tetrahedral Co(CO)₄⁻ configuration that are pertinent to crystalline charge-transfer salts. Furthermore, the tandem applications of the X-ray crystallographic and infrared spectroscopic results in Tables II and III reveal consistent patterns of Co(CO)₄⁻ distortions that are inherent to such inner-sphere (CIP) salts. Therefore the direct comparison of the carbonyl stretching bands in the IR spectra of crystalline Co(CO)₄⁻ salts with those found in tetrahydrofuran (or dichloromethane) solution establishes the same or closely related ion-pair structures to be extant in nonpolar solvents.

II. Charge-Transfer Spectra of CIP in the Solid State and in Solution. Most importantly, the variegated crystalline salts share, in common with their brightly colored solutions (Table I), the spectral characteristics of the charge-transfer transitions that are predicted by Mulliken theory (eq 5), as illustrated in Figure 2. Indeed the close relationship in Figure 11 between the diffuse reflectance spectra of crystalline salts with the absorption spectra of the salts dissolved in dichloromethane underscores the essential unity of the charge-transfer transitions ($h\nu_{\text{CT}}$) in the solid state and in solution. We therefore conclude that the critical interionic separations ($r_{\text{A}^+\text{D}^-}$) in Figures 3 and 4 are also pertinent to $h\nu_{\text{CT}}$ (eq 5) of these salts in solution.³¹ As such, the brightly colored solutions of charge-transfer salts derive directly from the contact ion pairs (CIP)—closely related in kind to those defined by X-ray crystallography and IR spectroscopy. Furthermore the charge-transfer spectrophotometry in Table V establishes such contact ion pairs to be the dominant species in nonpolar solvents (CH₂Cl₂, THF, etc); the solvatochromism in polar solvents (e.g., MeCN in Table IV) mainly relates to CIP dissociation in eq 7, as given by the distinctive change in the carbonyl IR bands.

III. Solvatochromism of Charge-Transfer Salts. The quantitative treatment of primary salt effects according to Figure 7 demonstrates that the charge-transfer salts of the type examined in this study are purely ionic salts, indistinguishable from the more commonly used electrolytes such as tetrabutylammonium perchlorate (TBAP) or hexafluorophosphate (TBAH).⁶⁸ Accordingly, the solvent effects on CIP dissociation to the solvent-separated ion pairs (SSIP) are our primary concern, since conductivity studies have shown that “free ions” are not particularly important

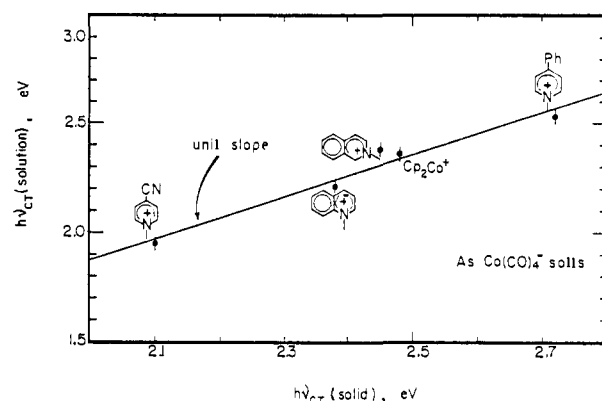


Figure 11. Direct correspondence of the charge-transfer transitions ($h\nu_{\text{CT}}$) of contact ion pairs (as indicated) in the solid state with those in dichloromethane solution. The line is arbitrarily drawn with a slope of unity.

in the aprotic solvents included in Table IV.⁴⁵ Nonetheless “free ions” are not distinguishable from SSIPs insofar as charge-transfer absorptions are observed in purely ionic salts.⁶⁹ This spectral differentiation (or lack thereof) does not apply to other charge-transfer salts, of which Tl⁺Co(CO)₄⁻ serves as the prime example.¹⁴ Thus, the elegant studies of Schramm and Zink have demonstrated that a wide spectrum of charge-transfer entities exist—extending from the nonionic, highly covalent TiCo(CO)₄ at one extreme through a series of contact and solvent-separated ion pairs, the relative importance of which is strongly modulated by solvent polarity. In marked contrast, such a direct coordination (of the metal) to the carbonylmetalate anion is precluded in metallocenium and pyridinium salts owing to their coordinatively saturated character.

Charge-transfer salts of the carbonylmetalates Co(CO)₄⁻, Mn(CO)₅⁻, and V(CO)₆⁻ bear a striking resemblance to the well-studied pyridinium iodides. Thus, the solvatochromism of metallocenium and pyridinium salts of this study are fundamentally related to that of the pyridinium iodides, as seminally established by Kosower.¹³ The use of carbonylmetalate donors [Co(CO)₄⁻, Mn(CO)₅⁻, V(CO)₆⁻, etc.] and metallocenium acceptors [Cp₂Co⁺, (C₆H₅)₂Cr⁺, etc.] does successfully extend the range of donor/acceptor properties to expand the solvatochromic scale.⁷⁰

IV. Mechanism of Charge-Transfer Photochemistry of Contact Ion Pairs. The charge-transfer salts of carbonylmetalates are distinguished from the iodide salts in the breadth of photochemistry that obtains upon exposure to visible light. For example, the continuous irradiation of the charge-transfer band ($\lambda \sim 350$ –500 nm) of the pyridinium iodides inflicts no permanent change of either the crystalline salt or that dissolved in CH₂Cl₂ or THF.⁷¹

(69) Aggregation of ion pairs is ignored. See: Goodson, B. E.; Schuster, G. B. *J. Am. Chem. Soc.* **1984**, *106*, 7254.

(70) For example, the solvatochromic shift of *N*-methyl-4-carbomethoxy-pyridinium iodide from 400 to 455 nm in MeCN and CH₂Cl₂ compares with the shift from 518 to 670 nm for Q⁺V(CO)₆⁻ in the same solvents (see Table IV).

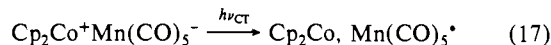
(67) Kosower, E. M. *Top. Curr. Chem.* **1983**, *112*, 117.

(68) See Gordon, J. E. in ref 4, p 55ff.

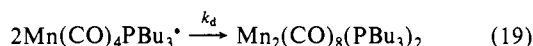
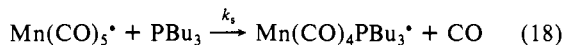
Moreover, the highly colored $\text{Co}(\text{CO})_4^-$, $\text{V}(\text{CO})_6^-$, and $\text{Mn}(\text{CO})_5^-$ salts are similarly unaffected by visible light for prolonged periods in the solid state or in solution. However, merely the presence of small amounts of additives L are sufficient to activate the carbonylmetalate salts to undergo a variety of distinctive photochemical reactions in solution.

At first glance, all of the photochemical processes described in Table VI are unique, with none showing any apparent stoichiometric relationship to the others. For example, the carbonylcobalt dimerization (eq 10) and disproportionation (eq 12) represent 1-electron oxidation processes of $\text{Co}(\text{CO})_4^-$, whereas the formation of $\text{Co}(\text{CO})_3\text{L}^-$ in eq 13 relates to a nonredox ligand substitution. The incorporation of the additive L into the carbonylmetal product, whether it be $\text{Co}_2(\text{CO})_6\text{L}_2$, $\text{Co}(\text{CO})_3\text{L}_2^+$, or $\text{Co}(\text{CO})_3\text{L}^-$ in eq 10, 12, and 13, respectively, is the sole feature that these photochemical processes have in common. Since the carbonylmetalates $\text{Co}(\text{CO})_4^-$, $\text{V}(\text{CO})_6^-$, and $\text{Mn}(\text{CO})_5^-$ are all thermally substitution-stable anions,⁷² the introduction of L into the carbonylmetalate moiety must occur in some reactive intermediate.

The time-resolved spectroscopic studies of the transient intermediates provide the keys to understanding the charge-transfer photochemistry of contact ion pairs. Thus the unambiguous identification of the carbonylmetal radical $\text{Mn}(\text{CO})_5^*$ immediately following the 10-ns laser-flash excitation of the contact ion pair $\text{Cp}_2\text{Co}^+\text{Mn}(\text{CO})_5^-$ at $\lambda = 532$ nm in Figure 8A relates directly to the photoredox process

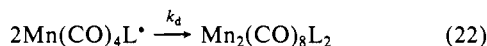
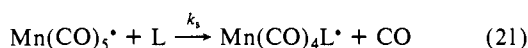
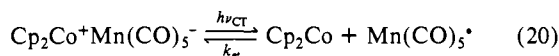


in accord with Mulliken theory.^{11,12} The concomitant production of cobaltocene in eq 17 could not be observed owing to its spectral overlap with the local absorptions of the separate ions Cp_2Co^+ and $\text{Mn}(\text{CO})_5^-$.^{21,22} Nonetheless, the persistence of the transient 800-nm band at times as short as 100 ns following the laser excitation,⁷³ coupled with the isolation of cobaltocene from the steady-state experiments (Table VI), represents the reasonable experimental verification of the Mulliken charge-transfer formulation. Most importantly, the enhanced reactivity of the 17-electron radical $\text{Mn}(\text{CO})_5^*$ leads to rapid ligand substitution by tributylphosphine and homolytic dimerization, i.e.



The large magnitudes of the rate constants k_s and $k_d = 1.0 \times 10^9$ and $1.0 \times 10^8 \text{ M}^{-1} \text{ s}^{-1}$, respectively, established by Brown and co-workers,^{74,60} are critical for the description of CT dimerization in eq 11, as given in the mechanistic scheme below. It is important to emphasize that the photoefficiency of CT dimerization according to Scheme I is generally dependent on the competition

Scheme I



between back electron transfer (k_{et}) and ligand substitution ($k_s\text{L}$). As such, the absence of photochemistry without added L derives from the facile back electron transfer of the initial radical pair, $\text{Mn}(\text{CO})_5^*$ and Cp_2Co , to regenerate the CIP in eq 20. Thus in order to account for the observed CT dimerization in Table VI

(71) For the photolysis of various ammonium iodide CT salts, see: (a) Kosower, E. M.; Lindqvist, L. *Tetrahedron Lett.* **1965**, 4481. (b) Ebbsen, T. W.; Ferraudi, G. *J. Phys. Chem.* **1983**, *87*, 3717. (c) Cozzens and Gover in ref 64.

(72) (a) Howell, J. A. S.; Burkinshaw, P. M. *Chem. Rev.* **1983**, *83*, 557. (b) Davison, A.; Ellis, J. E. *J. Organomet. Chem.* **1971**, *31*, 239. (c) Ungváry, F.; Wojcicki, A. *J. Am. Chem. Soc.* **1987**, *109*, 6848.

(73) By following the absorbance change at $\lambda_{\text{mon}} = 800$ nm.

(74) Herrinton, T. R.; Brown, T. L. *J. Am. Chem. Soc.* **1985**, *107*, 5700.

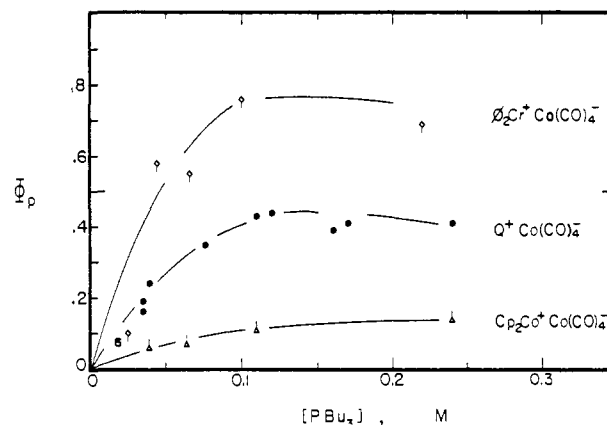
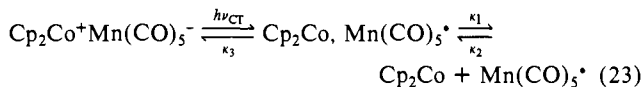


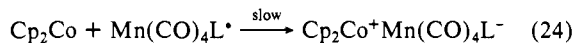
Figure 12. Limiting quantum yields for charge-transfer photochemistry of $\text{Co}(\text{CO})_4^-$ salts of various acceptor cations at increasing concentrations of the additive L = PBu_3 .

(entry 1), we estimate a value of $k_{\text{et}} < 10^8 \text{ s}^{-1}$, in order to allow competition for phosphine scavenging of $\text{Mn}(\text{CO})_5^*$ with $k_s = 1.0 \times 10^9 \text{ M}^{-1} \text{ s}^{-1}$ at roughly 0.1 M concentrations of added PBu_3 . Furthermore, the absence of CT photochemistry when the added PBu_3 is replaced with the less nucleophilic PPh_3 (see entry 13, Table VI) is a direct consequence of the mechanism in Scheme I, since the second-order rate constant for substitution $k_s = 1.7 \times 10^7 \text{ M}^{-1} \text{ s}^{-1}$ with L = PPh_3 is roughly 2 orders of magnitude slower than that with PBu_3 .⁷⁴

The kinetic results from the time-resolved experiments show that back electron transfer leading to annihilation of $\text{Mn}(\text{CO})_5^*$ actually proceeds by *second-order* kinetics, with the rate constant of $k_{\text{et}} = 3 \times 10^{10} \text{ M}^{-1} \text{ s}^{-1}$, as determined from the data in Table VIII (entries 1 and 2) together with the measured extinction coefficient of $\epsilon = 980 \text{ M}^{-1} \text{ cm}^{-1}$.⁶⁰ As such, any description of the photostationary state attained in the absence of additives must include the diffusive separation of the initial radical pair,⁷⁵ e.g.



where the measured rate constant $k_{\text{et}} \cong \kappa_2\kappa_3/\kappa_1$. Furthermore, the phosphine substitution of $\text{Mn}(\text{CO})_5^*$ to yield $\text{Mn}(\text{CO})_4\text{L}^*$ in eq 21 serves to enhance the photochemical efficiency by minimizing the energy-wasting back electron transfer, i.e.

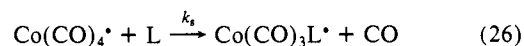
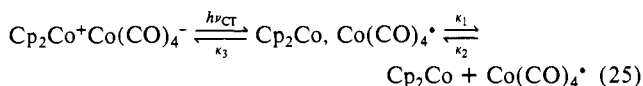


owing to the significantly attenuated reduction potentials of the phosphine-substituted radicals.⁷⁶

V. Selectivity in the CT Photochemistry of Contact Ion Pairs.

The time-resolved spectra in Figures 8B and 9 also accord with the Mulliken formulation for the photochemical activation of carbonylcobaltate salts. As such, the charge-transfer mechanism outlined for $\text{Mn}(\text{CO})_5^*$ should be generally applicable to the kindred 17-electron radical, i.e.

Scheme II

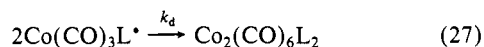


(75) Compare, e.g.: Koenig, T.; Fischer, H. In *Free Radicals*; Kochi, J. K., Ed.; Wiley: New York, 1973, Vol. 1, p 157ff. In this and the following discussion, we refer only to the second-order rate processes for $\text{Mn}(\text{CO})_5^*$ and $\text{Co}(\text{CO})_4^*$ as given in Table VIII. We hope that further time-resolved spectroscopy at the picosecond time scale will delineate the kinetics of the first-order cage return (κ_3).

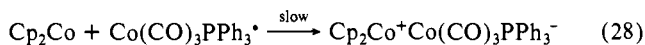
(76) (a) Kuchynka, D. J.; Amatore, C.; Kochi, J. K. *J. Organomet. Chem.* **1987**, *328*, 133. (b) The measured quantum yield $\Phi_p = 0.05$ in Table VII also indicates that the rate of back electron transfer in Scheme I is roughly 20 times faster than the rate of substitution (eq 21).

Indeed the cage mechanism in eq 25 is confirmed by the limiting value of the quantum yield, $\Phi_p(\text{limit})$ that is observed at high concentrations of added phosphine, as illustrated in Figure 12. According to Scheme II, the efficiency of CT photochemistry arises from the carbonylcobalt radicals $\text{Co}(\text{CO})_4^*$ that successfully undergo cage escape (κ_1) in competition with back electron transfer (κ_3). Importantly, the trend in the values of $\Phi_p(\text{limit})$ in the order $(\text{C}_6\text{H}_6)_2\text{Cr}^+ > \text{Q}^+ > \text{Cp}_2\text{Co}^+$ derives from the relative ease of electron back-transfer with the acceptor radicals $(\text{C}_6\text{H}_6)_2\text{Cr} < \text{Q}^* < \text{Cp}_2\text{Co}$, as based on the values of $E_c = -0.80, -0.90,$ and -0.95 V, respectively, in the Experimental Section. Most importantly however, there are specific elaborations to Scheme II that must be included to account for the unique product selectivities in charge-transfer dimerization, substitution, and disproportionation as they obtain with different phosphines described separately below.

A. Charge-Transfer Dimerization. We initially note that the second-order rate constant for back electron transfer (k_{et}) with $\text{Co}(\text{CO})_4^*$ appears to be an order of magnitude slower in Table VIII than that for $\text{Mn}(\text{CO})_5^*$ in Scheme I.⁷⁷ Secondly, the formation of the dimeric $\text{Co}_2(\text{CO})_6\text{L}_2$ with $\text{L} = \text{PPh}_3$ and PMe_2Ph in Table VI (entries 1 and 2) undoubtedly arises from the efficient scavenging of the carbonylcobalt radical (eq 26), followed by dimerization, i.e.

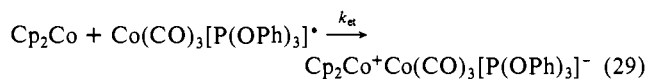


with the second-order rate constant $k_d > 10^5 \text{ M}^{-1} \text{ s}^{-1}$ and $k_{et} \sim 10^7 \text{ M}^{-1} \text{ s}^{-1}$ (see Experimental Section). Moreover, the energy-wasting back electron transfer of $\text{Co}(\text{CO})_4^*$ (with Cp_2Co) is obviated by the conversion to $\text{Co}(\text{CO})_3\text{PPh}_3^*$ whose annihilation, i.e.



is minimized as the result of its significantly reduced potential for reduction.⁷⁹ Indeed the quantum yield of $\Phi_p = 0.1$ for the CT dimerization of $\text{Cp}_2\text{Co}^+\text{Co}(\text{CO})_4^-$ with PPh_3 in Table VII indicates that $\text{Co}(\text{CO})_4^*$ undergoes ligand substitution roughly 10 times slower than back electron transfer in eq 25.

B. Charge-Transfer Substitution. Carbonylcobalt radicals are also critical intermediates when the phosphines PPh_3 and PMe_2Ph are replaced by the phosphite $\text{P}(\text{O}Ph)_3$ in Table VI (entry 4). The formation of $\text{Co}(\text{CO})_3[\text{P}(\text{O}Ph)_3]^-$ does not derive in eq 13 from direct ligand substitution, since $\text{P}(\text{O}Ph)_3$ is too weak a nucleophile to effect CO replacement in the substitution-inert $\text{Co}(\text{CO})_4^-$. However, the additives $\text{L} = \text{PPh}_3, \text{PMe}_2\text{Ph},$ and $\text{P}(\text{O}Ph)_3$ are strongly differentiated in the redox properties of the 17-electron intermediates $\text{Co}(\text{CO})_3\text{L}^*$ as formed in eq 26 (Scheme II). For example, the phosphite-substituted radical $\text{Co}(\text{CO})_3[\text{P}(\text{O}Ph)_3]^*$ is significantly more readily reduced than its phosphine analogue $\text{Co}(\text{CO})_3(\text{PMe}_2\text{Ph})^*$, the cathodic potentials at $E_c = -0.05$ and -0.45 V, respectively,^{79b} representing a difference of 9 kcal mol^{-1} . Coupled with the oxidation potential of -0.95 V for cobaltocene,⁸⁰ the driving force for back electron transfer



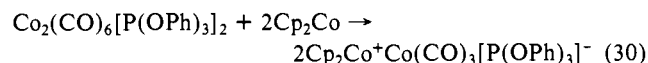
(77) (a) Assuming the extinction coefficient of $\text{Co}(\text{CO})_4^*$ at $\lambda_{\text{max}} = 780$ nm is comparable to that of $\text{Mn}(\text{CO})_5^*$. (b) However, the driving force for back electron transfer from $\text{Co}(\text{CO})_4^*$ is larger than that for $\text{Mn}(\text{CO})_5^*$.⁷⁸ It is possible that a possible discrepancy can be partly accounted for by a larger reorganization energy of $\text{Co}(\text{CO})_4^*$ (which is strongly distorted from the tetrahedral configuration^{63a}) relative to $\text{Mn}(\text{CO})_5^*$ (which suffers little change in geometry upon reduction⁶²). (c) For the comparative homolytic reactivity of cobalt(0) and manganese(0) species, see: Brown, T. L. and co-workers in ref 98.

(78) From cyclic voltammetry, $E_{1/2} = 0.05$ V for $\text{Mn}(\text{CO})_5^-$ by: (a) Kuchynka, D. J.; Kochi, J. K. *Inorg. Chem.* **1989**, *28*, 855. And $E_a = 0.32$ V (irrev) for $\text{Co}(\text{CO})_4^-$ at 500 mV s^{-1} by: (b) Mugnier, Y.; Reeb, P.; Moise, C.; Laviron, E. *J. Organomet. Chem.* **1983**, *254*, 111.

(79) (a) From cyclic voltammetry $E_a = 0.33$ and -0.28 V at 500 mV s^{-1} for $\text{Co}(\text{CO})_4^*$ and $\text{Co}(\text{CO})_3\text{PPh}_3^*$, respectively. (b) See: Lee, K. Y.; Kochi, J. K. in ref 58.

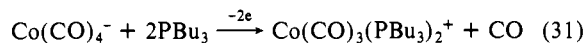
(80) Koelle, U. *J. Organomet. Chem.* **1978**, *152*, 225.

is estimated to be exergonic by $\Delta G \sim -20 \text{ kcal mol}^{-1}$. Although we were unable to directly measure the rate of electron transfer by time-resolved spectroscopy, we infer that $k_{et} > 10^8 \text{ M}^{-1} \text{ s}^{-1}$ from the large driving force for eq 29. Such large values of k_{et} leading to $\text{Cp}_2\text{Co}^+\text{Co}(\text{CO})_3[\text{P}(\text{O}Ph)_3]^-$ could thus be sufficient to obviate the formation of $\text{Co}_2(\text{CO})_6[\text{P}(\text{O}Ph)_3]_2$ via the bimolecular coupling of $\text{Co}(\text{CO})_3[\text{P}(\text{O}Ph)_3]^*$ in eq 27.⁸¹ The extent to which any of the dimeric $\text{Co}_2(\text{CO})_6[\text{P}(\text{O}Ph)_3]_2$ is formed will be subsequently reduced to the salt, i.e.



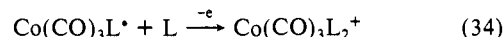
as shown by control experiments (see Experimental Section).

C. Charge-Transfer Disproportionation. The role of carbonylcobalt radicals in the conversion of $\text{Co}(\text{CO})_4^-$ to $\text{Co}(\text{CO})_3\text{L}_2^+$ was delineated in earlier electrochemical studies.⁸² Therefore let us consider the charge-transfer disproportionation of $\text{Cp}_2\text{Co}^+\text{Co}(\text{CO})_4^-$ in two distinct parts, namely, (a) the 2-electron oxidation of the anionic donor, i.e.

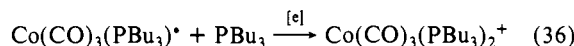
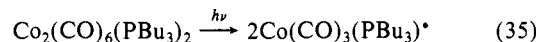


coupled with (b) the reduction of 2 equiv of Cp_2Co^+ , so that the combination of (a) and (b) represents the experimental stoichiometry in eq 12. The facile ligand substitution of carbonylcobalt radicals constitutes the pathway for the 2-electron transformation in eq 31, i.e.

Scheme III



which represents an electrochemical ECE mechanism.⁸² As such, transient electrochemical techniques differentiate phosphine ligands $\text{L} = \text{PPh}_3$ and PBu_3 by their effect on $\text{Co}(\text{CO})_3\text{L}_2^+$ —the redox potential of $\text{Co}(\text{CO})_3(\text{PBu}_3)_2^+$ being 0.61 V or 14 kcal mol^{-1} more favorable than that for $\text{Co}(\text{CO})_3(\text{PPh}_3)_2^+$.^{79b,83} The importance of such a redox property is also illustrated in the photodissociation^{63b} of $\text{Co}_2(\text{CO})_6(\text{PBu}_3)_2$ in the presence of both Q^+PF_6^- and PBu_3 . Separately, neither Q^+ nor PBu_3 has any perceptible effect on the photostationary state of $\text{Co}_2(\text{CO})_6(\text{PBu}_3)_2$ upon irradiation of the σ, σ^* band⁵⁷ with $\lambda \sim 380$ nm. However when both are present, essentially quantitative yields of $\text{Co}(\text{CO})_3(\text{PBu}_3)_2^+\text{PF}_6^-$ are obtained by a photoredox process that can be described as



where [e] represents the redox couple $[\text{A}^+ \rightarrow \text{A}^*]$ for the pyridinium acceptor A^+ .⁸⁶⁻⁸⁸ The importance of the latter is underscored in Table VI by the acceptor cations, which favor CT disproportionation in the following order: $\text{A}^+ = (\text{C}_6\text{H}_6)_2\text{Cr}^+ >$

(81) The value of $k_d = 10^8 \text{ M}^{-1} \text{ s}^{-1}$ estimated for $\text{Co}(\text{CO})_3[\text{P}(\text{O}Ph)_3]^*$ based on the analogy with the 17-electron carbonylmanganese species.⁶⁰

(82) (a) Reeb, P.; Mugnier, Y.; Moise, C.; Laviron, E. *J. Organomet. Chem.* **1984**, *273*, 247. See also: Lee, K. Y. in ref 79b.

(83) The oxidative substitution in eq 34 is likely to proceed stepwise by either (a) oxidation followed by ligand association⁸⁴ or (b) ligand association followed by oxidation.⁸⁵

(84) Rushman, P.; Brown, T. L. *J. Am. Chem. Soc.* **1987**, *109*, 3632.

(85) Stiegman, A. E.; Tyler, D. R. *Inorg. Chem.* **1984**, *23*, 527.

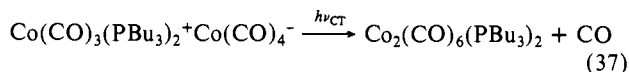
(86) For the analogous disproportionation of 17-electron carbonylmetal radicals that are photochemically generated from the direct homolysis metal-metal bonded dimer, see: Stiegman, A. E.; Tyler, D. R. *Coord. Chem. Rev.* **1985**, *63*, 217.

(87) (a) Carelli, I.; Cardinali, M. E.; Casini, A.; Arnone, A. *J. Org. Chem.* **1976**, *41*, 3967. (b) Kato, S.; Nakaya, J.; Imoto, E. *J. Electrochem. Soc. Jpn.* **1972**, *46*, 708. (c) Pyridinyl radicals formed in the CT photochemistry presumably dimerized,⁹⁷ although their fate was not established.

(88) Brown, T. L. *Ann. N.Y. Acad. Sci.* **1980**, *80*, 333. See also: References 60, 74, 84, and 86.

$Q^+ > Cp_2Co^+ > PP^+$. It is noteworthy that this also represents the decreasing trend in the reduction potentials of the cations in the same order, namely, $E_c = -0.80, -0.90, -0.95,$ and -1.22 V, respectively (see Experimental Section). A particularly dramatic influence of the cation is shown by the entirely different products obtained from the CT activation of $Cp_2Co^+Co(CO)_4^-$ and $Q^+Co(CO)_4^-$ in the presence of the same phosphine additive PMe_2Ph (compare entries 2 and 6, Table VI).

Finally, care must be exercised in the photochemical activation of contact ion pairs to irradiate only the charge-transfer absorption bands, and not those of the (colored) products. For example, the irradiation of either $Cp_2Co^+Co(CO)_4^-$ or $Q^+Co(CO)_4^-$ in the presence of PBu_3 at $\lambda > 510$ nm leads only to the dimeric $Co_2(CO)_6(PBu_3)_2$, despite the fact that the CT photochemistry of the same solution at $\lambda > 550$ nm leads smoothly to only the disproportionation products (Table VI, entries 4 and 7). In fact, control experiments demonstrate that the carbonylcobalt dimer arises from a secondary process by the adventitious excitation of the disproportionation salt, i.e.



Summary and Conclusion

The charge-transfer photochemistry of carbonylmetalate salts $A^+Mn(CO)_5^-$ and $A^+Co(CO)_4^-$ derives from contact ion pairs (CIP), whose structures are established by X-ray crystallography. These crystallographic structures can be successfully interrelated with contact ion pairs in solution by their characteristic carbonyl IR bands. Photoexcitation of the charge-transfer absorption band of the CIPs leads to the radical pairs $[A^*, Mn(CO)_5^*]$ and $[A^*, Co(CO)_4^*]$, which can be observed directly by time-resolved spectroscopy. Although prone to undergo facile back electron transfer, the radical pair can be scavenged by phosphine additives L in solution. The rapid ligand substitution of the 17-electron radicals $Mn(CO)_5^*$ and $Co(CO)_4^*$ gives rise to quantum-efficient photochemistry that is generally described as charge-transfer dimerization, disproportionation, and substitution according to the stoichiometries in eq 10, 12 and 13, respectively. The critical role of the phosphine ligand on the substituted carbonylmetal radicals, $Mn(CO)_4L^*$ and $Co(CO)_3L^*$, especially with regard to oxidation-reduction and coupling, is wholly consistent with their properties, principally delineated by Brown and co-workers from independent sources.⁸⁸ Moreover, the absence of significant CT photochemistry from carbonylvanadate salts $A^+V(CO)_6^-$ accords with ligand substitution rates of the corresponding 17-electron radical $V(CO)_6$ that are substantially slower⁸⁹ than those of $Mn(CO)_5^*$ and $Co(CO)_4^*$ in Table VIII. We hope that charge-transfer photochemistry of contact ion pairs can be further exploited in the mutual activation of nucleophile/electrophile pairs that are common in organic and organometallic chemistry.

Experimental Section

Materials. Dicobalt octacarbonyl (Strem), sodium hexacarbonylvanadate [as the bis(diglyme) stabilized salt, Strem], bis(benzene)chromium (Strem), and dimanganese decacarbonyl (Pressure Chemical) were used as received. Cobaltocene was prepared according to King.⁹⁰ Sodium tetracarbonylcobaltate was prepared from sodium hydroxide and dicobalt octacarbonyl in THF.⁹¹ Quinoline (Baker), isoquinoline (Matheson, Coleman and Bell), methyl isonicotinate (Aldrich), and 4-cyanopyridine (Aldrich) were used as received. Triphenylphosphine (Strem) was recrystallized from absolute ethanol. Tri-*n*-butylphosphine (Aldrich) and dimethylphenylphosphine (M and T Chemical) were distilled from sodium in vacuo. Triphenylphosphite (Aldrich) was stirred with CaH_2 overnight, decanted, and distilled in vacuo. The quaternary ammonium iodides were prepared by the general method detailed in Vogel.²⁴ The cobalt dimers $Co_2(CO)_6L_2$ ($L =$ phosphine or phosphite) were prepared by refluxing the ligand with $Co_2(CO)_8$ in benzene for several hours.⁵⁵ The salts $Co(CO)_3L_2^+Co(CO)_4^-$ ($L = PBu_3$ or $PPhMe_2$)

were prepared by the addition of the ligand L to a hexane solution of $Co_2(CO)_8$ at room temperature.⁹² The manganese dimer, $Mn_2(CO)_8$ (PBu_3)₂ was prepared by the method of Osborne and Stiddard.⁹³ The PPN^+ salts of $Co(CO)_4^-$ and $Mn(CO)_5^-$ were prepared from PPN^+Cl^- (Aldrich) by the methods of Ruff⁹⁴ and of Faltyněk and Wrighton,²¹ respectively.

Preparation of CT Salts of $Co(CO)_4^-$ with Pyridinium Cations. Sodium tetracarbonylcobaltate (0.19 g, 1.0 mmol) in deoxygenated water (20 mL) was stirred under an argon atmosphere at room temperature as a saturated solution of the pyridinium or quinolinium methiodide (1.0 mmol) in deoxygenated water was slowly added with the aid of an hypodermic syringe. The deeply colored CT salt immediately precipitated from the colorless mother liquor. It was removed by filtration under an argon atmosphere, liberally washed with deoxygenated water, and dried for 2–5 h in vacuo. The CT salt was washed into a Schlenk flask with a minimum volume of acetonitrile. Diethyl ether was added until crystallization began, and the solution was stored at $-20^\circ C$ overnight.

***N*-Methylquinolinium Tetracarbonylcobaltate [$Q^+Co(CO)_4^-$].** From 0.27 g (1.0 mmol) of Q^+I^- was obtained 0.24 g (78%) of $Q^+Co(CO)_4^-$ as deep red-purple crystals. IR (CH_3CN): ν_{CO} 1892 cm^{-1} . ¹H NMR (CD_3CN): δ 7.9–9.1 (m, 7 H), 4.52 (s, 3 H). Anal. Calcd for $C_{14}H_{10}NO_4Co$: C, 53.3; H, 3.2; N, 4.4. Found: C, 53.2; H, 3.2; N, 4.4.⁹⁵

***N*-Methyl-4-phenylpyridinium Cobaltate [$PP^+Co(CO)_4^-$].** From 0.30 g (1.0 mmol) of PP^+I^- was obtained 0.23 g (69%) of $PP^+Co(CO)_4^-$ as an orange powder. Anal. Calcd for $C_{16}H_{12}O_4NCo$: C, 56.3; H, 3.5; N, 4.1. Found: C, 55.6; H, 3.6; N, 4.0.

***N*-Methyl-4-cyanopyridinium Cobaltate [$NCP^+Co(CO)_4^-$].** From NCP^+I^- (0.25 g) was obtained 62% of $NCP^+Co(CO)_4^-$ as dark blue crystals. IR (CH_3CN): ν_{CO} 1894 cm^{-1} . Anal. Calcd for $C_{11}H_7N_2O_4Co$: C, 45.5; H, 2.4; N, 9.6. Found: C, 44.0; H, 2.5; N, 9.6.

***N*-Methylisoquinolinium Cobaltate [$iQ^+Co(CO)_4^-$].** From iQ^+I^- (0.27 g) was obtained 0.14 g (45%) of $iQ^+Co(CO)_4^-$ as bright red crystals. IR (CH_3CN): ν_{CO} 1892 cm^{-1} .

Cobaltocenium Cobaltate [$Cp_2Co^+Co(CO)_4^-$].⁹⁶ Dicobalt octacarbonyl (0.42 g, 1.2 mmol) was stirred at room temperature in benzene (20 mL) under an argon atmosphere. A solution of cobaltocene (0.50 g, 2.6 mmol) was prepared under an argon atmosphere in the same solvent (50 mL) and added to the $Co_2(CO)_8$ solution with the aid of a cannula. The dark brown crystalline precipitate that immediately formed was filtered under an argon atmosphere, washed with benzene, and dried in vacuo. Recrystallization from a mixture of THF and diethyl ether under an argon atmosphere yielded 0.50 g (58%) of dark red crystals. IR (CH_3CN): ν_{CO} 1892 cm^{-1} . ¹H NMR (CD_3CN): δ 5.56 (cp H). Anal. Calcd for $C_{14}H_{10}O_4Co_2$: C, 46.7; H, 2.8. Found: C, 46.6; H, 2.8.

Bis(benzene)chromium Cobaltate [$(C_6H_6)_2Cr^+Co(CO)_4^-$]. The analogous treatment of $Co_2(CO)_8$ (1.2 mmol) in benzene with a solution of bis(benzene)chromium (0.52 g, 2.5 mmol) in benzene yielded a black crystalline precipitate. Recrystallization from a mixture of THF and diethyl ether yielded 0.40 g (43%) of black crystals. IR (CH_3CN): ν_{CO} 1892 cm^{-1} . Anal. Calcd for $C_{16}H_{12}O_4CoCr$: C, 50.6; H, 3.2. Found: C, 50.6; H, 3.2.

Cobaltocenium Manganate [$Cp_2Co^+Mn(CO)_5^-$]. To a solution of cobaltocene (4.6 g, 24 mmol) in 50 mL of benzene under an argon atmosphere was added dropwise with stirring a solution of bromine (1.9 g, 11.8 mmol) in pentane (50 mL) over a period of 1 h. After the addition, the mixture was stirred for 1 h and the solution concentrated. The dark green precipitate was dissolved in MeCN (100 mL) and the solution was rapidly filtered through a bed of Celite. The volume of MeCN was reduced to 20 mL, and ethyl acetate (80 mL) was added to precipitate the product. Yield, 0.9 g. IR (KBr): 1412 (s), 1115 (s), 856 (s), 503 (s), 466 (s) cm^{-1} . The yellow solid, which was not characterized further, was dissolved in 10 mL of CH_3CN . A solution of $Na^+Mn(CO)_5^-$ was prepared by stirring $Mn_2(CO)_{10}$ (0.68 g, 1.7 mmol) with sodium amalgam (0.7 g Na, 40 g Hg) in THF (30 mL) under an argon atmosphere. The greenish-yellow suspension was filtered through a bed of Celite directly into the acetonitrile solution of Cp_2CoBr . Filtration through a bed of Celite removed the white precipitate (NaBr). After the solvent was removed in vacuo, the reddish-brown solid was transferred to the dry box and recrystallized from a mixture of THF and diethyl ether. $Cp_2Co^+Mn(CO)_5^-$ was washed with ether to remove the residual $Mn_2(CO)_{10}$, and it afforded 0.35 g of the reddish-brown crystalline solid. IR (acetone): ν_{CO} 1902, 1864 cm^{-1} . The preparation of the hexacarbonylvanadate salts followed the method of Calderazzo et al.¹⁵ with slight modifications.

(89) Shi, Q. Z.; Richmond, T. G.; Togler, W. C.; Basolo, F. *J. Am. Chem. Soc.* **1984**, *106*, 71.

(90) King, R. B. *Organometallic Synthesis*; Academic: New York, 1965; Vol. 1, p 70.

(91) Edgell, W. F.; Lyford, J., IV *Inorg. Chem.* **1970**, *9*, 1932.

(92) Hieber, W.; Freyer, F. *Chem. Ber.* **1958**, *91*, 1230.

(93) Osborne, A. G.; Stiddard, M. H. B. *J. Chem. Soc.* **1964**, 634.

(94) Ruff, J. K. *Inorg. Synth.* **1972**, *15*, 87.

(95) Elemental analyses by Atlantic Microlabs, Norcross, GA.

(96) Chini, P.; Albano, V.; Martinengo, S. *J. Organomet. Chem.* **1969**, *16*, 471.

Typically, a solution of bis(diglyme) sodium hexacarbonylvanadate (0.50 g, 1.02 mmol) in deoxygenated water (25 mL) was stirred under an argon atmosphere at room temperature while the appropriate pyridinium iodide (1.0 mmol) was added as a degassed saturated aqueous solution. The dark-colored precipitate was filtered under an argon atmosphere, washed with water, and dried in vacuo at room temperature for 2–5 h. Unsatisfactory elemental analyses⁹⁵ were obtained for these compounds owing to their thermal instability even in the solid state. However, the IR and UV spectra of the freshly prepared crystal were similar to those reported.¹⁵ For example, $\text{Q}^+\text{V}(\text{CO})_6^-$. IR (THF): ν_{CO} 2021 (vw), 1900 (m, br), 1858 (vs) cm^{-1} ; (CH_3CN) ν_{CO} 1860 (vs) cm^{-1} . $\text{CMP}^+\text{V}(\text{CO})_6^-$. IR (THF): ν_{CO} 2021 (vw), 1902 (m, br), 1858 (vs) cm^{-1} ; (CH_3CN) ν_{CO} 1860 (vs) cm^{-1} . $\text{Cp}_2\text{Co}^+\text{V}(\text{CO})_6^-$. Vanadium hexacarbonyl (0.40 g, 1.8 mmol) prepared by the method of Ellis et al.^{72b} was dissolved in 20 mL of diethyl ether under an inert atmosphere. A solution of 0.5 g (2.6 mmol) of cobaltocene in diethyl ether (70 mL) was added slowly and the dark green crystalline precipitate was washed repeatedly with ether until the washings were colorless. The solid was dried in vacuo to give 0.41 g (55%) of $\text{Cp}_2\text{Co}^+\text{V}(\text{CO})_6^-$. IR (THF): ν_{CO} 2021 (vw), 1900 (sh), 1853 (vs) cm^{-1} ; (CH_3CN) ν_{CO} 1859 (vs) cm^{-1} . UV-vis (10^{-3} M CH_2Cl_2): 355 nm (ϵ 8000), 410 (850), 600 (400).

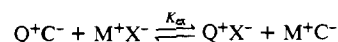
$\text{Cp}_2\text{Co}^+\text{I}^-$. To a suspension of cobaltocene (2.98 g, 16 mmol) in benzene (30 mL) under an argon atmosphere was added dropwise a solution of iodine (2.0 g, 7.8 mmol) in benzene (100 mL). The suspension was stirred for 2 h and filtered in air. This precipitate was recrystallized twice from a mixture of acetonitrile and ethyl acetate to yield 2.63 g (53%) of yellow crystals. Samples were prepared for X-ray crystallography by dissolving ~ 10 mg into acetonitrile contained in a small vial. The vial was placed inside a 100-mL round-bottom flask containing some diethyl ether, and the capped flask was allowed to stand. Vapor diffusion at room temperature produced golden-yellow plates which were mounted for X-ray crystallography. IR (KBr): 3058 (s), 1824 (m), 1414 (s), 1113 (s), 1065 (br), 859 (s), 500 (s), 462 (vs) cm^{-1} .⁹⁷ Crystals of $\text{Q}^+\text{Co}(\text{CO})_4^-$, $\text{Cp}_2\text{Co}^+\text{Co}(\text{CO})_4^-$, and $\text{NCP}^+\text{Co}(\text{CO})_4^-$ were similarly grown for X-ray crystallography by vapor-phase diffusion. Typically, the CT salt (~ 5 mg) was dissolved in THF, and the small vial was placed in a 50-mL Erlenmeyer flask containing diethyl ether. The flask was closed and cooled to -25 °C. After 24 h crystallization was apparent. The crystals were collected, washed with diethyl ether, and dried in a stream of dry nitrogen. Crystalline samples were stored at -25 °C under nitrogen until mounted in the diffractometer.

Instrumentation. Infrared spectra were measured on a Nicolet 10DX FT-IR spectrometer. All measurements of liquid samples were made with 1.0 mm NaCl cells. Solvent absorptions were compensated for by digital subtraction. Solid samples were measured in KBr disks. Solution UV-vis spectra were recorded on a Hewlett-Packard 8450-A diode-array spectrometer. Crystalline CT salts were recorded as 10% dispersions in silica gel. The diffuse reflectance spectra were recorded on a Perkin-Elmer 330-A spectrometer equipped with a Hitachi H210-2101 integrating sphere accessory using an alumina disk as the reference. ^1H NMR spectra were recorded on a JEOL FX90Q FT NMR spectrometer operating at 89.55 MHz.

UV-vis Spectroscopy of Charge-Transfer Salts. Solvents for spectrophotometry were purified and stored under an argon atmosphere. Acetonitrile (Fisher) was allowed to stand with 0.1% KMnO_4 overnight, and the mixture was refluxed for 1 h. The brown MnO_2 residue was removed by filtration. The acetonitrile was fractionally distilled from P_2O_5 and then redistilled from CaH_2 . Butyronitrile (Eastman) was passed through activated (Woelm Super-1) alumina and degassed by three freeze-pump-thaw cycles. Dichloromethane (Baker) and chloroform (Mallinckrodt) were each distilled from P_2O_5 and redistilled from CaH_2 . Tetrahydrofuran (THF, Fisher) was distilled from sodium and then from lithium aluminum hydride. Diethyl ether (Fisher) was distilled from a mixture of sodium and benzophenone. Acetone (Fisher) was fractionally distilled from P_2O_5 . Tetra-*n*-butylammonium perchlorate (TBAP, Aldrich) was recrystallized from ethyl acetate and hexane and dried overnight at room temperature in vacuo. All spectroscopic measurements were made under an argon atmosphere in a UV cell equipped with a Teflon valve. Owing to their instability, the spectral properties of the vanadate salts were measured immediately after preparation.

Salt Effects on the Solution Spectra of Charge-Transfer Salts. A solution of the CT salt in CH_2Cl_2 (2×10^{-3} M) was prepared in a 1-cm quartz cuvette. The UV-vis spectrum was acquired, an aliquot of a stock solution of TBAP in CH_2Cl_2 (0.2 M) added, and the spectrum remeasured. Since the total volume change arising from the multiple additions of the stock solution was less than 10%, no correction was applied. Results were plotted as the relative decrease in the absorbance at the CT maximum ($A_{\text{CT}}/(A_{\text{CT}})_0$) versus the mole fraction of CT salt, as shown

in Figure 7. The quantitative relationship between the CT absorption and the salt concentration can be derived for the equilibrium



where Q^+C^- is the CT salt and M^+X^- is the inert salt (complete ion-pairing assumed). The equilibrium constant is expressed as $K_{\text{ex}} = [\text{Q}^+\text{X}^-][\text{M}^+\text{C}^-]/[\text{Q}^+\text{C}^-][\text{M}^+\text{X}^-]$. If we let C_{QC} and C_{MX} be the formal concentrations of the CT salt and the inert salt, respectively, and apply the mass-balance restriction, it follows that $K_{\text{ex}} = (C_{\text{QC}} - [\text{Q}^+\text{C}^-])^2/[\text{Q}^+\text{C}^-](C_{\text{MX}} - C_{\text{QC}} + [\text{Q}^+\text{C}^-])$. When $K_{\text{ex}} = 1$, this equation simplifies to $[\text{Q}^+\text{C}^-] = (C_{\text{QC}})^2/(C_{\text{QC}} + C_{\text{MX}})$. Since only Q^+C^- absorbs light, $[\text{Q}^+\text{C}^-]$ is also the absorbance divided by the extinction coefficient and therefore, $A_{\text{CT}}/\epsilon_{\text{CT}} = (C_{\text{QC}})^2/(C_{\text{QC}} + C_{\text{MX}})$. In the absence of added salt, $A_{\text{CT}} = (A_{\text{CT}})_0 = \epsilon_{\text{CT}}C_{\text{QC}}$ and $(A_{\text{CT}})/(A_{\text{CT}})_0 = C_{\text{QC}}/(C_{\text{QC}} + C_{\text{MX}})$ in accord with the unit slope in Figure 7.

Dissociation Constants of Charge-Transfer Salts. The method of Drago and Rose⁵⁰ as modified by Schramm and Zink¹⁴ was used for the determination of K_{CT} in eq 8. Concentrations of the CT salts that ranged from 5×10^{-4} to 1×10^{-2} M in THF and CH_2Cl_2 , and from 5×10^{-3} to 11×10^{-2} M in CH_3CN , were prepared and the spectra recorded. Curves were plotted for the apparent dissociation constant as a function of trial values of the extinction coefficient according to the modified eq 8, where A_{CT} represents CT absorbance at λ_{max} , C represents the concentration of the CT salt, and ϵ_{CT} represents the trial values of the extinction coefficient. The intersections of the curves were averaged and reported as ϵ_{CT} and K_{CT} in Table V.

Charge-Transfer Photochemistry of CT Salts. Photolyses were performed with the focused light from a Hanovia 450-W xenon lamp that was passed through an IR filter and an appropriate glass sharp cutoff filter (λ_{cutoff} 520 or 550 nm, Corning CS-3). The temperature in the Schlenk tube was controlled with an unsilvered Dewar flask filled with water at room temperature. An argon atmosphere was maintained throughout the photolysis and subsequent sampling.

$\text{Cp}_2\text{Co}^+\text{Co}(\text{CO})_4^-$ and PPh_3 . A solution of the CT salt (0.054 g, 0.15 mmol) and triphenylphosphine (0.078 g, 0.3 mmol) in 5 mL of CH_2Cl_2 was irradiated for 8 h at $\lambda > 520$ nm. During the irradiation, a reddish-brown precipitate formed. The red precipitate was collected and identified by its IR spectrum as $\text{Co}_2(\text{CO})_6(\text{PPh}_3)_2$. Yield 0.040 g (65%). IR (KBr): 3057 (w), 1950 (vs), 1481 (s), 1431 (s), 1306 (m), 1187 (m), 1159 (m), 1096 (s), 1031 (m), 997 (m), 743 (s), 709 (s), 690 (s), 547 (s), 515 (vs) cm^{-1} . No change was observed in the IR spectrum of a CH_2Cl_2 solution of $\text{Cp}_2\text{Co}^+\text{Co}(\text{CO})_4^-$ and PPh_3 that was allowed to stand in the dark for 24 h. Recovery of cobaltocene: A mixture of $\text{Cp}_2\text{Co}^+\text{Co}(\text{CO})_4^-$ (0.054 g) and triphenylphosphine (0.078 g) was photolyzed for 9 h in 5 mL of THF. The dark supernatant solution was filtered under an argon atmosphere, the THF was removed in vacuo, and cobaltocene was removed from the residue by sublimation at 50–60 °C onto a cold finger cooled with dry ice. After 3 h, the sublimation tube was transferred to the glovebox and the crystals were removed to yield 18 mg (63%) of cobaltocene. IR (KBr): 3082 (m), 2921 (m), 1772 (w), 1690 (w), 1565 (w), 1415 (m), 1105 (m), 994 (s), 778 (vs) cm^{-1} , identical with authentic cobaltocene.

$\text{Cp}_2\text{Co}^+\text{Co}(\text{CO})_4^-$ and PBu_3 . A mixture of the CT salt (0.11 g 0.30 mmol) and PBu_3 (0.10 g, 0.52 mmol) was photolyzed for 6 h in ($\lambda > 520$) in THF until no further change was observed in the IR spectrum. The solvent was removed in vacuo and cobaltocene was sublimed onto a cold finger as described above. Yield, 0.023 g (41%).

$\text{Q}^+\text{Co}(\text{CO})_4^-$ and PBu_3 . The CT salt (0.13 g, 0.41 mmol) was photolyzed in 25 mL of THF containing 81 mg (0.40 mmol) of PBu_3 . After 4 h of photolysis, the color of the solution faded from dark purple to light yellow, and the IR spectrum of the solution showed no further change. Analysis of the carbonyl band at 1988 cm^{-1} indicated a 95% yield of $\text{Co}(\text{CO})_3(\text{PBu}_3)_2^+\text{Co}(\text{CO})_4^-$. The solvent was reduced in volume to 2 mL, and the addition of diethyl ether (10 mL) precipitated the product. Dissolution of the precipitate in CH_2Cl_2 (3 mL) followed by reprecipitation with ether yielded 0.11 g (76%) of $\text{Co}(\text{CO})_3(\text{PBu}_3)_2^+\text{Co}(\text{CO})_4^-$. IR (KBr): 2961 (m), 2934 (m), 2872 (m), 1997 (vs), 1981 (vs), 1882 (vs), 1461 (m), 1385 (m), 1219 (m), 1097 (m), 1057 (w), 971 (w), 908 (m), 799 (w), 733 (w), 573 (m), 554 (s), 497 (m) cm^{-1} , which was identical with the IR spectrum of material prepared from $\text{Co}_2(\text{CO})_8$ and PBu_3 .⁵⁸ Other photoreactions were analyzed by IR spectroscopy without recourse to the isolation of the carbonylcobalt product. In a typical reaction, a solution of the CT salt and an excess of the additive L was irradiated (using either the 520- or 550-nm cutoff filter, vide supra). The course of the photoreaction was monitored by periodically extracting an aliquot for IR analysis. Irradiation was continued until the IR spectrum either showed no further change or the initially formed products began to decompose. Products were identified and quantified by IR spectroscopy of their principal carbonyl components. Calibration of $\text{Cp}_2\text{Co}^+\text{Co}(\text{CO})_3[\text{P}(\text{O}Ph)_3]^-$ was performed with solution prepared by the in situ

(97) Van den Akker, M.; Jellinek, F. *Recl. Trav. Chim.* 1971, 90, 1101.

reduction of $\text{Co}_2(\text{CO})_6[\text{P}(\text{O}(\text{Ph})_3)_2]$ with excess cobaltocene (assuming complete conversion to the anion).

$\text{Cp}_2\text{Co}^+\text{Co}(\text{CO})_4^-$ and PBu_3 . Photolysis of a THF solution containing 0.010 M CT salt and 0.015 M PBu_3 for 1.5 h yielded $\text{Co}(\text{CO})_3(\text{PBu}_3)_2^+$ (ν_{CO} 1998 and 1988 cm^{-1} , 60%) and $\text{Co}_2(\text{CO})_6(\text{PBu}_3)_2$ (ν_{CO} 1943 cm^{-1} , 15%).

$\text{Cp}_2\text{Co}^+\text{Co}(\text{CO})_4^-$ and PMe_2Ph . Photolysis of the CT salt (0.004 M) in THF with excess phosphine (0.008 M) for 3 h resulted in the conversion to the bis(phosphine)-substituted dimer (ν_{CO} 1949 cm^{-1} , 50% yield).

$\text{Cp}_2\text{Co}^+\text{Co}(\text{CO})_4^-$ and $\text{P}(\text{O}(\text{Ph})_3)_3$. Photolysis of 0.010 M CT salt with an equimolar amount of $\text{P}(\text{O}(\text{Ph})_3)_3$ in THF led to formation of the substituted anion [ν_{CO} 1960 (m), 1879 (s), 1861 (s) cm^{-1}] in 60% yield. A trace of $\text{Co}_2(\text{CO})_6[\text{P}(\text{O}(\text{Ph})_3)_2]$ (ν_{CO} 1981 cm^{-1}) was also observed.

$\text{Q}^+\text{Co}(\text{CO})_4^-$ and $\text{P}(\text{O}(\text{Ph})_3)_3$. Irradiation of a mixture of the CT salt (0.003 M) and $\text{P}(\text{O}(\text{Ph})_3)_3$ (0.007 M) in THF (3 mL) for 3 h resulted in a color change from purple to brownish red. Infrared spectroscopy showed the presence of only $\text{Co}_2(\text{CO})_6[\text{P}(\text{O}(\text{Ph})_3)_2]$ in 80% yield (ν_{CO} 1981 cm^{-1}).

$\text{Q}^+\text{Co}(\text{CO})_4^-$ and PMe_2Ph . The CT salt (0.014 M) and ligand (0.020 M) were photolyzed for 1.5 h, during which time the color of the solution changed from purple to light brown. Infrared spectroscopy revealed a prominent band at 2001 cm^{-1} , identical with that of authentic $\text{Co}(\text{CO})_3(\text{PMe}_2\text{Ph})_2^+$ as the $\text{Co}(\text{CO})_4^-$ salt (90%). A trace of dimer (ν_{CO} 1955 cm^{-1}) was also detected.

$\text{PP}^+\text{Co}(\text{CO})_4^-$ and PBu_3 . This CT salt (0.008 M) in THF was irradiated in the presence of PBu_3 (0.024 M). After photolysis for 1.5 h, the concentration of $\text{Co}_2(\text{CO})_6(\text{PBu}_3)_2$ reached a maximum. A yield of dimer (corresponding to 22% of the starting material) was calculated from the absorbance measured at 1943 cm^{-1} . No absorption was noted at 1998 or 1988 cm^{-1} , corresponding to cationic product.

$(\text{C}_6\text{H}_5)_2\text{Cr}^+\text{Co}(\text{CO})_4^-$ and PBu_3 . From a solution of this salt in THF (0.010 M) containing excess ligand (0.020 M), only cationic product was observed in 19% yield (ν_{CO} 1998 and 1988 cm^{-1}).

$(\text{C}_6\text{H}_5)_2\text{Cr}^+\text{Co}(\text{CO})_4^-$ and PMe_2Ph . A similar irradiation for 2.5 h of a THF solution of the CT salt (0.006 M) only gave the cation in low yield (16%).

$\text{Cp}_2\text{Co}^+\text{Mn}(\text{CO})_5^-$ and PBu_3 . Irradiation of the CT salt (0.012 M) with PBu_3 (0.070 M) in acetone for 2 h led to a 16% yield of $\text{Mn}_2(\text{CO})_8(\text{PBu}_3)_2$ (ν_{CO} 1943 cm^{-1}). Continued irradiation resulted in no further change in the infrared spectrum of the solution.

$\text{Cp}_2\text{Co}^+\text{Mn}(\text{CO})_5^-$ and PPh_3 . The CT salt (0.012 M) was photolyzed in acetone containing PPh_3 (0.070 M) for 7 h at $\lambda > 520$ nm and room temperature. No change was observed in either the UV or IR spectrum during this time.

$\text{Cp}_2\text{Co}^+\text{V}(\text{CO})_6^-$ and PPh_3 or PMe_3 . Irradiation of the CT salt (0.004 M) in THF with either PPh_3 or PMe_3 (0.007 M) resulted in no change in the UV-vis or IR spectrum over a 7-h period.

Photolysis of $\text{Co}_2(\text{CO})_6(\text{PBu}_3)_2$ in the Presence of Q^+PF_6^- and PBu_3 . A solution of 2.8 mg (0.004 mmol) of the dimer, dissolved in 2 mL of CH_2Cl_2 was photolyzed ($\lambda > 380$) for 1 h. No change in the infrared (1943 cm^{-1}) spectrum was observed. An excess (7.7 mg, 0.027 mmol) of *N*-methylquinolinium hexafluorophosphate was added and the solution was photolyzed again. No change in the IR spectra was observed. Tributylphosphine (8.0 mg, 0.04 mmol) was added, and photolysis for 45 min resulted in complete conversion of $\text{Co}_2(\text{CO})_6(\text{PBu}_3)_2$ as noted by the disappearance of the carbonyl band at 1943 cm^{-1} . The solvent was removed in vacuo and replaced with THF (2.0 mL). Quantitative IR analysis at 1988 cm^{-1} was used to determine the yield of $\text{Co}(\text{CO})_3(\text{PBu}_3)_2^+$ as 0.008 mmol (quantitative). Photolysis of $\text{Co}_2(\text{CO})_6(\text{PBu}_3)_2$ (2×10^{-3} M) with excess PBu_3 for 1 h under the same conditions without Q^+PF_6^- afforded no change in the IR spectrum.

Thermal Reactions of Dimeric $\text{Co}_2(\text{CO})_6\text{L}_2$ with Cobaltocene. Cobaltocene (19 mg, 0.10 mmol) was added to a solution of $\text{Co}_2(\text{CO})_6[\text{P}(\text{O}(\text{Ph})_3)_2]$ (45 mg, 0.05 mmol) in THF (5 mL) at room temperature. The IR spectrum of the reaction mixture taken immediately after mixing showed the disappearance of the strong carbonyl band at 1981 cm^{-1} of the dimer. Three new bands appeared at ν_{CO} = 1960 (m), 1879 (s), and 1860 (sh) cm^{-1} . [Lit.⁸² for $\text{Co}(\text{CO})_3[\text{P}(\text{O}(\text{Ph})_3)_2]^+$, ν_{CO} 1960 (m), 1876 (s), 1863 (sh)]. Repetition of the experiment, with $\text{Co}_2(\text{CO})_6(\text{PPh}_3)_2$ (40 mg, 0.05 mmol) for 3 h showed no change in the carbonyl IR band of $\text{Co}_2(\text{CO})_6(\text{PPh}_3)_2$ at ν_{CO} 1957 cm^{-1} .

Quantum Yields for the Charge-Transfer Photochemistry. A 450-W xenon lamp equipped with a narrow band pass interference filter (550 \pm 5 nm, Edmund Scientific) was employed as the monochromatic light source. The light intensity was measured with a Reinecke salt actinometer.⁵⁶ Typically, the solutions consisted of 9–16 mM CT salt and 0.010–0.24 M tributylphosphine in THF. A 3.0-mL aliquot was transferred to the argon-flushed cuvette, and the contents were irradiated with stirring. An aliquot of the stock solution (1.0 mL) was allowed to stand

in the dark as the control. At the end of irradiation (1–3 h), the solution was reexamined by IR spectroscopy. The concentration of $\text{Co}(\text{CO})_3(\text{PBu}_3)_2^+$ was determined by comparison with a calibration curve based on $\text{Co}(\text{CO})_3(\text{PBu}_3)_2^+\text{Co}(\text{CO})_4^-$. For the manganese salt, authentic $\text{Mn}_2(\text{CO})_8(\text{PBu}_3)_2$ was used to calibrate the IR cell. Quantum yields were expressed as $\Phi_p = [\mu\text{mol of } \text{Co}(\text{CO})_3(\text{PBu}_3)_2^+ \text{ produced}] / [\mu\text{einstein of light absorbed}]$. Minor transmission corrections (<20%) were applied in those cases where the absorbance at $\lambda = 550$ nm was less than 2.0. The CT salt, added L, and Φ are given serially as follows: (a) [$\text{Q}^+\text{Co}(\text{CO})_4^-$] (mM), [PBu_3] (M), Φ_p : 9.0, 0.018, 0.08; 9.0, 0.018, 0.07; 8.8, 0.035, 0.19; 8.8, 0.035, 0.16; 9.8, 0.029, 0.24; 9.5, 0.076, 0.35; 10.2, 0.12, 0.43; 9.5, 0.11, 0.44; 9.7, 0.17, 0.42; 8.9, 0.16, 0.39; 9.5, 0.23, 0.40; (b) [$\text{Cp}_2\text{Co}^+\text{Co}(\text{CO})_4^-$] (mM), [PBu_3] (M), Φ_p : 14.0, 0.039, 0.06; 9.0, 0.060, 0.07; 13.1, 0.11, 0.11; 13.2, 0.24, 0.14; (c) [$(\text{C}_6\text{H}_5)_2\text{Cr}^+\text{Co}(\text{CO})_4^-$] (mM), [PBu_3] (M), Φ_p : 13.7, 0.025, 0.10; 11.6, 0.046, 0.58; 12.6, 0.066, 0.55; 16.9, 0.10, 0.76; 15.0, 0.22, 0.69; (d) [$\text{Cp}_2\text{Co}^+\text{Mn}(\text{CO})_5^-$ in acetone] (mM), [PBu_3] (M), Φ_p : 24, 0.060, 0.05.

Time-Resolved Spectroscopy of Charge-Transfer Salts. The CT salt was placed in the Schlenk tube under an argon atmosphere, and dichloromethane or acetone was added with the aid of a hypodermic syringe. The concentration was adjusted to yield an absorbance of ~ 0.5 at $\lambda = 532$ nm. The solution was frozen with liquid nitrogen and degassed by freezing and thawing in vacuo four times. A 2.0-mL aliquot of the solution was transferred under an argon atmosphere to a fluorometer cell equipped with a Teflon valve. The UV-vis spectra were acquired before and after the flash photolysis to check for decomposition. Flash photolysis was performed with a Quantel YG 580-10 Q-switched Nd-YAG laser (10-ns pulse width) frequency-doubled to 532 nm. The full laser output of 150–160 mJ was reduced to lower power by a series of copper screen filters. A 150-W Xe lamp provided the interrogating light that was passed through a monochromator (Oriol 77250) equipped with an Oriol 77298 diffraction grating (300–1000 nm) to a Hamamatsu R9128 photomultiplier tube. Transient acquisition was performed with a Tektronix 7104 oscilloscope in conjunction with a Tektronix C101 digitizing video camera. Acquisition sequences were controlled by a Kinetic Instruments KI-1 sequence generator and laser controller. Transients were recorded and processed with an AT&T 6300-plus microcomputer using Tektronix DC501 software. Transient spectra were acquired by successive photolyses and the change of the monochromator in 10-nm steps. The scan range was limited to the 350–900-nm range by the interrogating lamp intensity. Strong ground-state absorptions of Cp_2Co^+ prevented the spectral observations at $\lambda < 450$ nm. The decay kinetics were based on the averages of 16–20 transients. The reaction order was established by linear least-squares computer fit of the observed decrease in the absorbance with time as a function of either $\ln A$ or A^{-1} for first or second order, respectively. In each case, the random distribution of the residuals over 3–4 half-lives was used for the kinetics order, and it allowed a ready discrimination between simple first- and second-order decays. Photolyses of $\text{Cp}_2\text{Co}^+\text{Mn}(\text{CO})_5^-$ and $\text{Q}^+\text{Co}(\text{CO})_4^-$ were performed at varying laser intensities to establish with certainty that the derived first- or second-order rate constant was invariant.

Flash Photolysis of $\text{Co}_2(\text{CO})_8$. A solution of $\text{Co}_2(\text{CO})_8$ (5×10^{-5} M) in hexane was made up under an argon atmosphere in a Schlenk cell. The contents were degassed by four freeze-pump-thaw cycles. Carbon monoxide was admitted and the solution was photolyzed at 355 nm (using the second harmonic of the Nd-YAG laser). The carbonyl bands at 350 and 460 nm of $\text{Co}_2(\text{CO})_8$ were bleached and a weak transient appeared at 550 nm. When the sample was degassed and argon readmitted, only the transient at $\lambda = 550$ nm persisted. From the bleaching kinetics, the restoration of $\text{Co}_2(\text{CO})_8$ occurred with a second-order rate constant of $7.9 \times 10^9 \text{ M}^{-1} \text{ s}^{-1}$. No transient at $\lambda = 780$ nm was noted. Since some of the rate constants for the dimerization and ligand substitution of the 17-electron radicals are unknown, their magnitudes were estimated as follows: The values of k_d were taken from the published literature as 9×10^8 , 1×10^8 , and $1 \times 10^7 \text{ M}^{-1} \text{ s}^{-1}$ for $\text{Mn}(\text{CO})_5^+$, $\text{Mn}(\text{CO})_4\text{PBu}_3^+$, and $\text{Mn}(\text{CO})_4\text{PPh}_3^+$, respectively,⁶⁰ and $k_d = 4 \times 10^8$ and $9 \times 10^7 \text{ M}^{-1} \text{ s}^{-1}$ for $\text{Co}(\text{CO})_4^+$ and $\text{Co}(\text{CO})_3\text{PBu}_3^+$, respectively.^{63b} The value of $k_d = 9 \times 10^6 \text{ M}^{-1} \text{ s}^{-1}$ was estimated for $\text{Co}(\text{CO})_3\text{PPh}_3^+$ by assuming the same substituent effect as that observed for $\text{Mn}(\text{CO})_4\text{L}^+$ above. By an analogous reasoning, we could only proceed from the reported values of $k_s = 1 \times 10^9$ and $2 \times 10^7 \text{ M}^{-1} \text{ s}^{-1}$ for ligand substitution of $\text{Mn}(\text{CO})_5^+$ by PBu_3 and PPh_3 , respectively.⁷⁴ If $k_s > 10^7 \text{ M}^{-1} \text{ s}^{-1}$ for the substitution of $\text{Co}(\text{CO})_4^+$ by PBu_3 ,⁹⁸ then $k_s > 10^5 \text{ M}^{-1} \text{ s}^{-1}$ can be estimated for the ligand substitution of $\text{Co}(\text{CO})_4^+$ by PPh_3 by taking a similar substituent effect.

Electrochemistry of Acceptor Cations and Carbonylmetal Anions. The electrochemistry of the cations and anions used in this study was per-

formed in acetonitrile. The supporting electrolyte, tetra-*n*-butylammonium hexafluorophosphate (TBAH, G. F. Smith), was recrystallized from ethyl acetate and dried at 100 °C in vacuo. The CV cell was equipped with Teflon valves and viton O-rings to ensure an air- and grease-free anolyte. Solutions of the anolyte (5.0×10^{-3} M) and TBAH (0.10 M) were prepared in the cell by standard Schlenk techniques. Cyclic voltammetry was performed with an *iR*-compensated potentiostat⁵⁸ that was driven by a Princeton Applied Research Model-175 Universal Programmer. Potentials were referenced to an aqueous SCE connected to the anolyte compartment via a cracked glass tip. The value of $E_{1/2} = 0.95$ V for cobalticenium was used as the reference.⁸⁰ For the cations, the reversible $E_{1/2}$ values of PP^+ , Cp_2Co^+ , $(C_6H_6)_2Cr^+$, CMP^+ , and NCP^+ were observed at -1.22, -0.95, -0.80, -0.76, and -0.64 V at $v = 500$ mV s⁻¹. The irreversible cathodic wave E_c of Q^+ and iQ^+ at -0.90 and -1.08 V at $v = 500$ mV s⁻¹ compared with the values of $E_c = -1.27$, -0.99, -0.79, and -0.67 V for PP^+ , Cp_2Co^+ , CMP^+ , and NCP^+ , respectively, under the same conditions. For the anions, the irreversible anodic wave E_a of I^- , $Co(CO)_4^-$, $V(CO)_6^-$, and $Mn(CO)_5^-$ occurred at 0.36, 0.33, 0.06, and -0.11 V at $v = 500$ mV s⁻¹ in acetonitrile.

X-ray Crystallography of Charge-Transfer Salts. $Cp_2Co^+Co(CO)_4^-$. A blood-red triangular crystal ($0.50 \times 0.30 \times 0.15$ mm) was mounted on a glass fiber in a random orientation on a Nicolet R3m/V automatic diffractometer. The radiation was Mo $K\alpha$ monochromatized ($\lambda = 0.71073$ Å) by a highly ordered graphite crystal. The final cell constants, as well as other information pertinent to data collection and refinement were as follows: space group $C2/c$ (monoclinic) with cell constants $a = 9.414$ (2), $b = 10.761$ (2), $c = 14.306$ (3) Å; $\beta = 99.94$ (2)°; $V = 1428$ Å³; chemical formula $C_{14}H_{10}O_4Co_2$; fw 360.1; $Z = 4$; $\rho = 1.68$ g cm⁻³; $\mu = 23.27$ cm⁻¹; $I > 3\sigma(I)$ 1118; $R = 0.037$; $R_w = 0.022$ with $w = \sigma/(F)^2$, $R = \sum(|F_o| - |F_c|)/\sum|F_o|$ and $R_w = [\sum(|F_o| - |F_c|)^2/\sum w|F_o|^2]^{1/2}$. The Laue symmetry was determined to be $2/m$, and from the systematic absences noted, the space group was shown to be either Cc or $C2/c$. Intensities were measured by the θ - 2θ scan technique, with the scan rate depending on the count obtained in rapid prescans of each reflection. Two standard reflections were monitored after every 2 h or every 100 data collected, and these showed a 6% linear decay over the 32 h of the experiment. A normalizing factor as a function of exposure time was used to account for this. In reducing the data, Lorentz and polarization corrections were applied, as well as an empirical absorption correction based on ψ scans of 10 reflections having χ values between 70 and 90°. Since the cation involved is capable of lying on an inversion center or a 2-fold axis and the anion could have 2-fold symmetry, the space group was initially assumed to be the centrosymmetric $C2/c$. The structure was solved by the Patterson interpretation program of SHELXTL, which gave the positions of the two cobalt atoms in the asymmetric unit, consisting of half of each molecule. As expected, the cation lies on an inversion center (resulting in staggered Cp ligands) while the anion lies on a 2-fold axis. The usual sequence of isotropic and anisotropic refinement was followed, after which all hydrogens were entered in ideal calculated positions. A single nonvariable isotropic thermal parameter was assigned to all of the hydrogen atoms. After all shift/esd ratios were less than 0.1, convergence was reached at the agreement factors listed above. No unusually high correlations were noted between any of the variables in the last cycle of full-matrix least-squares refinement, and the final difference density map showed no peaks greater than 0.30 e Å⁻³. All calculations were made with Nicolet's SHELXTL PLUS series of crystallographic programs.⁹⁹

$Q^+Co(CO)_4^-$. A large burgundy multifacet polyhedron ($0.50 \times 0.30 \times 0.18$ mm) was mounted on the diffractometer as described above. The final cell constants and other crystallographic data were as follows: space group $C2/c$ (monoclinic) with cell constants $a = 18.534$ (3), $b = 11.837$ (2), $c = 13.951$ (2) Å; $\beta = 114.87$ (1)°; $V = 2777$ Å³; chemical formula $C_{14}H_{10}O_4NCo$; fw 315.2; $Z = 8$; $\rho = 1.51$ g cm⁻³; $\mu = 12.4$ cm⁻¹; $I > 3\sigma(I)$ 1760; $R = 0.033$; $R_w = 0.030$. The Laue symmetry was determined to be $2/m$, and the space group was shown to be either $C2/c$ or Cc . Intensities were measured by the ω scan technique, with the scan rate depending on the count obtained in rapid prescans of each reflection. The structure was solved by use of the SHELXTL Patterson interpretation program,⁹⁹ which revealed the position of the cobalt atom. The remaining non-hydrogen atoms were located in subsequent difference Fourier syntheses. Aromatic hydrogens were added at ideal calculated positions and held fixed; however, the methyl hydrogens were located in Fourier maps and allowed to refine independently. After all shift/esd ratios were less than 0.1, convergence was reached at the agreement factors listed

above. No unusually high correlations were noted between any of the variables in the last cycle of full-matrix least-squares refinement, and the final difference density map showed no peak greater than 0.2 e Å⁻³.

$NCP^+Co(CO)_4^-$. A small, black cherry trapezoidal prism of ($0.22 \times 0.15 \times 0.09$ mm) was treated as above. Space group $Pbca$ (orthorhombic) with cell constants $a = 12.052$ (3), $b = 15.248$ (4), $c = 13.647$ (4) Å; $V = 2508$ Å³; chemical formula $C_{11}H_7O_4N_2Co$; fw 290.13; $Z = 8$; $\rho = 1.54$ g cm⁻³; $\mu = 13.7$ cm⁻¹; $I > 3\sigma(I)$ 846; $R = 0.041$; $R_w = 0.029$. The Laue symmetry was determined to be mmm , and from the systematic absences noted, the space group was shown unambiguously to be $Pbca$. Intensities were measured by the ω scan technique. The structure was solved by interpretation of the Patterson map, which revealed the position of the Co atom. The remaining non-hydrogen atoms were located in subsequent difference Fourier syntheses. Hydrogens were added in ideal calculated positions and held fixed. The C10 methyl group was allowed to rotate as a rigid body, so as to correctly position the hydrogens with respect to the pyridine plane. After all shift/esd ratios were less than 0.3, convergence was reached at the agreement factors listed above.

$Cp_2Co^+V(CO)_6^-$. A small black parallelepiped of $0.45 \times 0.20 \times 0.15$ mm was mounted as described above. Space group $C2$ (monoclinic) with cell constants $a = 12.369$ (7), $b = 8.719$ (4), $c = 7.872$ (4) Å; $\beta = 101.01$ (4)°; $V = 833$ Å³; chemical formula $C_{16}H_{10}O_6CoV$; fw 408.13; $Z = 2$; $\rho = 1.63$ g cm⁻³; $\mu = 15.6$ cm⁻¹; $I > 3\sigma(I)$ 692. However, owing to the massive disorder of $V(CO)_6^-$ in the crystal, the refinement was not carried to completion. Moreover $Cp_2Co^+V(CO)_6^-$ packed in at least one other extremely intricate arrangement and aged poorly.

$Cp_2Co^+I^-$. A large orange-yellow square plate ($0.45 \times 0.45 \times 0.12$ mm) was mounted as described above. The final cell constants and other crystallographic data were as follows: space group $I422$ (tetragonal) with cell constants $a = 6.719$ (2), $c = 11.668$ (4) Å; $V = 527$ Å³; chemical formula $C_{10}H_{10}CoI$; fw 316.03; $Z = 2$; $\rho = 1.99$ g cm⁻³; $\mu = 44.7$ cm⁻¹; $I > 3\sigma(I)$ 218; $R = 0.069$; $R_w = 0.069$. The Laue symmetry was determined to be $4/mmm$, and from the systematic absences noted, the space group was shown to be $I422$, $I4mm$, $I4m2$, $I42m$, or $I4/mmm$. Since the cell constants indicated only two molecules per unit cell, it was immediately evident that in any of the above space groups the cyclopentadienes would have to be heavily disordered. Therefore after data collection a second, much thinner plate was mounted in order to verify the cell constants and Laue group. Intensities were measured by the θ - 2θ scan technique. In reducing the data, Lorentz and polarization corrections were applied, as well as an empirical absorption correction based on ψ scans of seven reflections having χ values between 70 and 90°. Since all five possible space groups presuppose heavy disorder, $I422$ was arbitrarily chosen for initial refinement. The structure was solved by use of the SHELXTL direct methods program, which revealed the positions of the Co and I atoms. The unitary structure factors displayed acentric statistics, although little weight was placed on this due to the suspected disorder. The Cp carbon atoms were located in subsequent Fourier syntheses and were found to be close to the c axis, which means that both rings have to be disordered over at least four different positions about a common centroid. Essentially, the rings appear as toroids of electron density, and thus for the sake of convenience a rigid body model was used, with each carbon having a population factor of 25%. Refinements in each of the other four space groups resulted in almost identical R values; however, the planes of the two Cp rings about Co showed somewhat larger deviations from parallelism than in the $I422$ refinement. Therefore the final refinement was made in $I422$, although none of the other four space groups can be categorically excluded. After all shift/esd ratios were less than 0.1, convergence was reached at the agreement factors listed above. The only unusually high correlation noted between any of the variables in the last cycle of full-matrix least-squares refinement involved the z coordinate of the rigid body Cp ring and one of its rotational variables. The final difference density map showed a maximum peak of ~ 1.0 e Å⁻³, located quite close to the iodine atom.

Acknowledgment. We thank the National Science Foundation (CHE-8716570), the Texas Advanced Research Program (1056-ARP), and the Robert A. Welch Foundation for financial support. We also thank J. D. Korp for crystallographic assistance, S. Sankararaman for helpful suggestions, and the National Science Foundation for funds to construct the laser flash spectrometer.

Supplementary Material Available: Tables of atomic coordinates and equivalent isotropic displacement parameters (of non-hydrogen atoms) for $Cp_2Co^+Co(CO)_4^-$, $Q^+Co(CO)_4^-$, $NCP^+Co(CO)_4^-$ and $Cp_2Co^+I^-$ (2 pages). Ordering information is given on any current masthead page.

(99) Sheldrick, G. M. *SHELXTL PLUS Programs for Crystal Structure Determination*; Nicolet XRD Corp.: Madison, WI, 1987.